HIGH TEMPORAL RESOLUTION CARBONATE CHEMISTRY AT THE EAST FLOWER GARDEN BANK

A Thesis

by

VANCE SCOTT NYGARD

Submitted to the Office of Graduate and Professional Studies of
Texas A&M University
in partial fulfillment of the requirements for the degree of

MASTER OF SCIENCE

Chair of Committee,	Niall C. Slowey
Committee Members,	Richard S. Mercier
	Kathryn E. Shamberger
Head of Department,	Shari Yvon-Lewis

August 2018

Major Subject: Oceanography

ABSTRACT

Understanding and predicting the consequences of ocean acidification for current coral reef communities necessitate high-frequency baseline data. This study presents two months of carbonate chemistry parameters measured *in situ* every two hours and discrete samples taken at the East Flower Garden Bank in the Northwest Gulf of Mexico. Daily trends of temperature, chlorophyll-a (Chl-a), pH, dissolved oxygen (DO), pressure, and photosynthetically active radiation (PAR) are presented and discussed. Cross-correlations between the parameters' cycles show their relative timing. Relative Hourly Variability, a composite coefficient of variation, describes the regularity of daily cycles over time. Seasonal changes of aragonite saturation state (Ω_{arag}), dissolved inorganic carbon, and normalized total alkalinity (nTA) and the aforementioned parameters are compared to historical data from the same site and match well with measurements made at coral reefs of comparable latitude.

Typical daily trends of less than 0.75 C, 0.05 pH units, 0.9 mL L^{-1} DO, and 0.6 mg m^{-3} Chl-a are observed. PAR largely peaks at 10 or noon local time, and the closely correlated DO and pH consistently peak 2-4 hours thereafter. The timing of the temperature cycle is inconsistent. From early May to early July, temperature (3.3 C) and pCO_2 (58 ppm) increase; pH decreases by 0.047 units on the total scale; salinity, nTA, and Ω_{arag} remain largely unchanged. These trends correlate well with those observed during congruent seasons at HOTS, ESTOC, and BATS (Bates et al. 2014). As a relatively deep and exposed reef, the East Flower Garden Bank is a valuable addition to the existing literature of coral reef carbonate chemistry.

DEDICATION

To the Wife and little ‘Laide.

ACKNOWLEDGEMENTS

Dr. Kathryn Shamberger of the Department of Oceanography and Dr. Richard Mercier of the Department of Civil Engineering provided thoughtful advice and direction instrumental to the successful completion of this research. The staff of the Flower Garden Banks National Marine Sanctuary deserve high praise for their professionalism, hospitality, and scientific assistance, especially John Embesi, Marissa Nuttall, G.P. Schmahl, Emma Hickerson, Travis Stern, and Michelle Johnston. Thanks to Drs. Ruth Perry of the Shell Oil Company and Rebecca Green of the Bureau of Ocean Energy Management for their roles in the conception and direction of the research project and good conversations about the chlorophyll data. Thanks also to Dr. Xinping Hu of Texas A&M University – Corpus Christi and Dr. Benjamin Giese of Texas A&M University for helpful discussions. Eddie Webb, John Walpert, and co-workers at the Geochemical and Environmental Research Group at TAMU provided invaluable assistance.

Thanks also go to my friends, colleagues, and the department faculty (especially Dr Christina Wiederwohl) and staff for making my time at Texas A&M University a great experience. Special gratitude is due to Dr. Niall Slowey for his passion, direction, detailed attention, and unwavering support during a long and intense project.

Finally, thanks beyond words to my mother and father for their encouragement. Most importantly, my thanks go to my wife for her patience, offspring, faith, and love.

Soli Deo Gloria.

CONTRIBUTORS AND FUNDING SOURCES

This work was supported by a thesis committee consisting of Dr. Niall Slowey [advisor] and Dr. Kathryn Shamberger of the Department of Oceanography and Dr. Richard Mercier of the Department of Civil Engineering.

The data analyzed for the TAMU Cruise was provided by Andrea Kealoha. The discrete water sample analyses were conducted at Texas A&M University in part by GERG and in part by the Shamberger Lab.

All work for the thesis was completed by the student under the advisement of and in collaboration with his advisor Dr. Niall Slowey.

Graduate study was supported by Bureau of Ocean Energy Management (BOEM) Cooperative Agreement M14AC00028, Shell Exploration Production Award M410560, scholarships from Texas A&M University, and NSF Grant 1355807 S-STEM Scholars in Oceanography.

NOMENCLATURE

CDOM	Chromophoric Dissolved Organic Matter (mg m^{-3})
Chl-a	Chlorophyll-a Fluorescence (mg m^{-3})
DO	Dissolved Oxygen (mL L^{-1})
EFGB	East Flower Garden Bank
FGBNMS	Flower Garden Banks National Marine Sanctuary
PAR	Photosynthetically Active Radiation (mmol $m^{-2}s^{-1}$)
	Pressure (dbar)
	Salinity (psu)
	Temperature (ITS-90, deg C)
	Turbidity (NTU)

TABLE OF CONTENTS

Page

LIST OF FIGURES

Page

LIST OF TABLES

Page

1 INTRODUCTION

The natural steady-state CO_2 concentrations in the atmosphere and oceans are being disturbed by carbon emissions from anthropogenic processes such as fossil fuel use and cement production (e.g. Keeling 1973; Feely et al. 2004). The atmosphere has gained roughly 100 ppm CO_2 over the last 60 years (Keeling et al. 2007). Between a quarter and a third of the yearly increase in atmospheric CO_2 dissolves into the oceans (Sabine et al. 2004; Canadell 2007). Among the most quantifiable and ecologically important effects of the current increase of carbon dioxide concentrations is the phenomenon of ocean acidification – the decrease of seawater's pH caused by the dissolution of atmospheric carbon dioxide. Important implications of this ongoing dissolution include decreases of pH and carbonate ion concentration and increases of dissolved inorganic carbon and pCO_2 (Feely et al. 2010). As more CO_2 dissolves into the ocean, its capacity to buffer both acid-base equilibria and future CO_2 fluxes diminishes (e.g. Sabine et al. 2004). Not only these physical processes, but many biological entities will be affected.

One especially important type of marine ecosystem particularly threatened by ocean acidification is the coral reef. Coral reefs are ecologically important and economically valuable (worth billions of dollars in yearly values of fisheries, tourism, biodiversity and coastal protection) ecosystems found throughout the world (e.g. Moberg and Folke 1999; Cesar et al. 2003; Cinner and Kittinger 2015). Warming, eutrophication, de-oxygenation, increased stratification, and other drivers are documented stressors of coral communities (see Riebesell and Gattuso 2015 and references therein). Coral skeletons are composed of calcium carbonate ($CaCO_3$), and much of the seafloor surrounding individual corals on a reef is covered with detrital $CaCO_3$ fragments from corals and a wide variety of other organisms. Corals and other calcifying marine species will find the calcification process increasingly difficult due to ocean

acidification's effects (e.g. Schneider and Erez 2006). (The typical measure for the $CaCO_3$ saturation of seawater is Ω, which is discussed in-depth in the Seawater Carbonate Chemistry section below.) Calcification requires carbonate ions, and the ocean's decreasing pH decreases its carbonate ion concentration ($[CO_3^{-2}]$), which is expected to hamper the calcification of tropical corals (Chan and Connally 2013; Comeau et al. 2013).

Despite the potentially deleterious effects of ocean acidification, long-term, high temporal resolution monitoring of oceanic pH levels and carbonate mineral saturation state is sparse. Although there are seven stations measuring annual cycles of carbonate chemistry parameters – and some since 1983 – only two measure pH directly, and even the highest temporal resolution does not exceed 16 samples per year (Bates et al. 2014). Until recently, oceanographers have encountered challenges with deploying and retaining well-calibrated pH meters in the ocean for extended periods of time. pH is a dynamic water property, varying widely among different water masses, in different hydrographical conditions, and with changing seasons (e.g. Wanninkof et al. 2015). Thus, it is critical to better study how pH and its associated parameters change along with environmental processes during the daily, weekly, and seasonal timespans.

As explained in the Seawater Carbonate Chemistry section below, any two of the following parameters can be used to calculate the others: pH, pCO_2, total alkalinity (TA), and dissolved inorganic carbon (DIC). While discrete samples could be taken and analyzed for each parameter, it may not be feasible to collect the number of desired field samples when high temporal resolution is desired. An alternative approach is to measure pH and other components of the carbonate chemistry system simultaneously *in situ*.

We have developed an integrated system of sensors capable of collecting high-quality, high temporal resolution measurements of pH and other environmental parameters that influence the carbonate saturation state of seawater. The seafloor component of this system was deployed within meters of live corals at the crest of the East Flower Garden Bank (EFGB), a thriving and ecologically significant subtropical coral reef located at the outer edge of the continental shelf in the northwestern Gulf of Mexico (Fig. 1). We present here an evaluation of measurements made at two hour intervals over a period of two months and consider their significance relative to daily variations, weekly patterns, and seasonal trends.

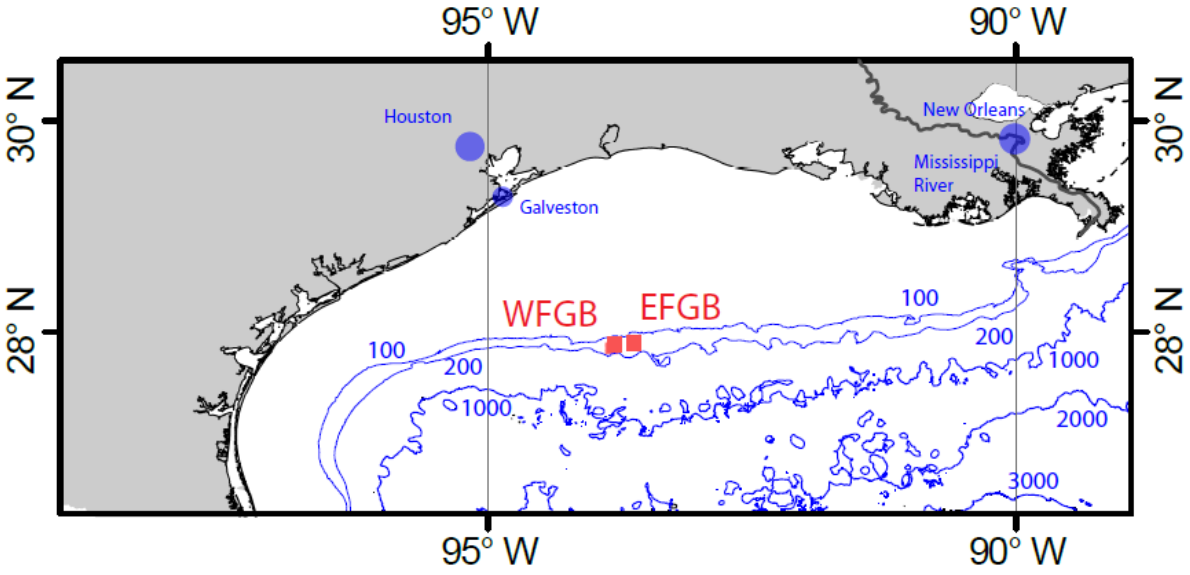

Fig. 1 Location of FGBNMS in the northwestern Gulf of Mexico. This coral reef is situated at the continental shelf-slope break between the 100 and 200 m depth contours (blue lines).

2 MARINE ENVIRONMENTAL SETTING

The coral reefs on the East Flower Garden Banks, which are within the National Oceanographic and Atmospheric Administration (NOAA) Flower Garden Banks National Marine Sanctuary (FGBNMS), are considered to be among the Gulf of Mexico's healthiest and ecologically significant coral ecosystems. Centered at 27.9° N and 93.6° W, they are one of the highest latitude tropical reefs found in the world's oceans and exhibit a surprisingly high degree of coral cover for that latitude (Liddell and Ohlhorst 1988). They are home to more than 30 species of corals that occur throughout the Caribbean Sea, Gulf of Mexico, and other areas. Well-studied coral genera include *Acropora, Porites, Montastrea*, *Orbicella*, and *Siderastrea*, and others such as *Agaricia*, *Colpophyllia* and *Millepora* are common (Bright et al. 1984; Rezak et al. 1985; FGBNMS staff, personal communication). Some other commonly found fauna are rays, sharks, and approximately 170 species of fish (Gittings 1997). The FGBNMS was designated a "priority geographic area" by NOAA in its National Coral Reef Monitoring Plan (NOAA Coral Program 2014).

Located ~190 km offshore of Galveston, Texas, at the outer edge of the Texas-Louisiana continental shelf, the coral communities at the East Flower Garden Banks (EFGB) are well situated for the study of the Gulf of Mexico's environmental conditions (Fig. 1). At this distance from the coast, the banks are minimally influenced by either coastal anthropogenic influences or the runoff of the Mississippi-Atchafalaya River System (Rezak et al. 1990), and its waters are generally representative of near-surface open-ocean Gulf water (Rezak et al. 1985; Wagner and Slowey 2011). The EFGB's coral cap covers about 67 km^2 (Rezak et al. 1983), lying about 21 m below the sea surface on the peaks of a salt diapir (Bright et al. 1984), which rises ~80 m above the surrounding seafloor (Fig. 2). At this depth, the reef is buffered from the dynamic sea

surface; nevertheless, short-term events may influence the reef, such as when the passage of cold fronts during winter cools waters on the broad continental shelf (Nowlin and Parker 1974; Slowey and Crowley 1995) or, possibly, upwelling or strong mixing events bring waters from deeper depths up over the shelf-slope break. Its location on the shelf-slope break exposes EFGB to potentially vigorous shelf edge ocean circulation, giving this site a habitat that is simultaneously indicative for the entire marginal sea and unique for coral reef research.

How might the pH and other environmental parameters that influence the carbonate saturation state of seawater vary at the Flower Garden Banks? Well-ventilated waters from the open Gulf of Mexico and the Caribbean Sea circulate through the gulf and across the Flower Garden Banks (Rezak et al. 1985; Jochens and DiMarco 2008; Teague et al. 2013). Takahashi et al. (2009) calculated a climatological mean annual sea–air CO_2 flux (g Carbon m^{-2} yr^{-1}) of near zero in the northwestern Gulf of Mexico, which implies the CO_2 system values of surface water should reliably reflect the influence of atmospheric conditions.

This study site has a comparable latitude (27.9° N) to three other sites, where similar seasonal trends are expected. The Hawaii Ocean Time-series (HOT; 22° 45’ N; Dore et al. 2009), Bermuda Atlantic Time-series Study (BATS; 32° N; Bates et al. 2012) and European Station for Time series in the Ocean at the Canary Islands (ESTOC; 29.04° N; González-Dávila et al. 2010) show over the months of May and June a decrease in pH, an increase of pCO_2, a steady or slightly increasing Ω_{arag} (Fig. 2 in Bates et al. 2014).

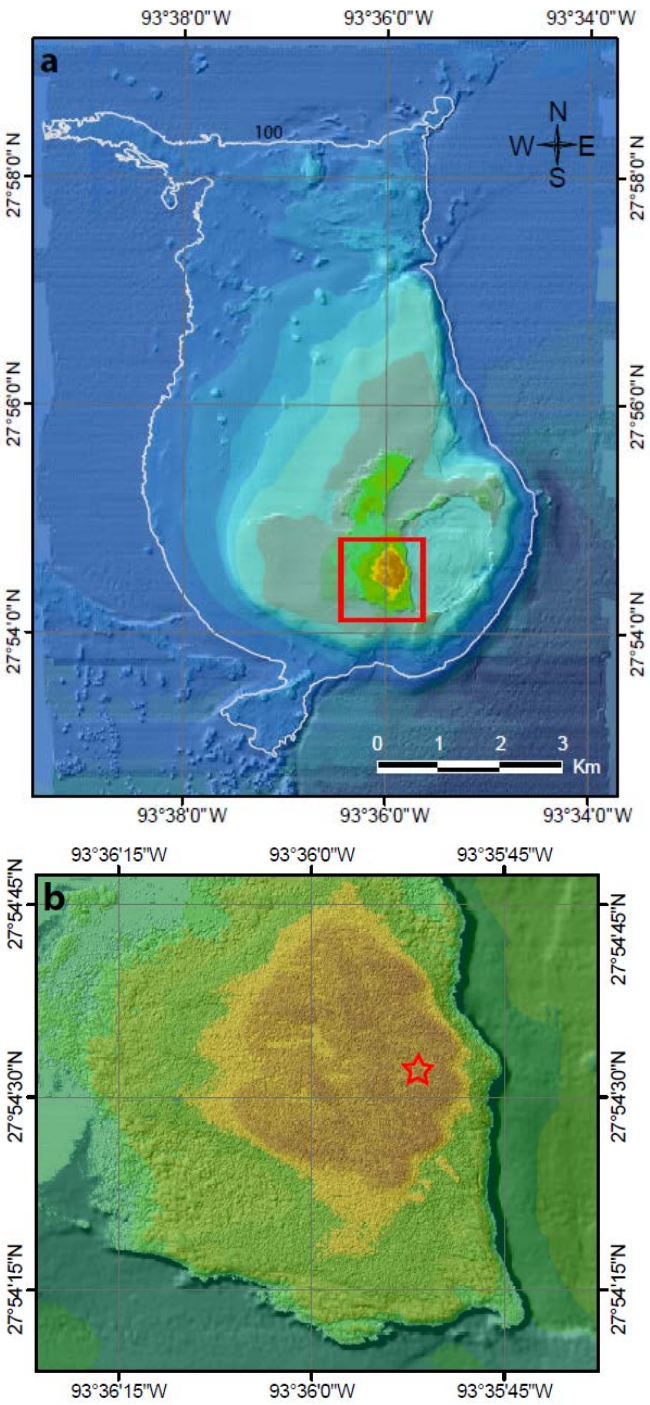

Fig. 2 a) Seafloor bathymetry surrounding East Flower Garden Bank. The white contour indicates 100 m water depth and the color variations indicate 10 m water depth intervals. **b)** The details of area within the red box in **a**. The red star indicates the location where the sensor package was deployed.

3 SEAWATER CARBONATE CHEMISTRY

Several important aspects of seawater's carbonate system are reviewed here. For further details see reviews by Broecker and Peng 1982; Morse and MacKenzie 1990; Dickson et al. 2007; and Andersson 2014.

Gaseous carbon dioxide dissolves into the ocean, where it reacts with water to form carbonic acid.

$$CO_2\,(g) \leftrightarrow CO_2\,(aq) + H_2O \leftrightarrow H_2CO_3$$

Carbonic acid quickly dissociates into a hydronium ion (i.e. acid; commonly expressed as H^+) and bicarbonate. The latter can further dissociate into carbonate and another hydronium ion.

$$H_2CO_3 \leftrightarrow HCO_3^- + H^+ \leftrightarrow CO_3^{-2} + 2H^+$$

All components of the carbonate chemistry system coexist in varying concentrations in seawater.

Carbonic acid is not the only source of acid in the ocean: other acid-base systems based on ammonium, boron, phosphate, nitrate, nitrite, sulfide, silicate, fluoride and sulfate contribute to the overall presence of hydronium ions (Hagens and Middelburg 2016). The total acidity of an aqueous solution (pH) is expressed as:

$$pH = -log[H^+]$$

The primary chemical components of the ocean's pH are of the carbonic acid family; thus, a global decrease in oceanic pH levels associated with the anthropogenic increase of atmospheric CO_2 is already being measured, and this decrease is expected to continue (e.g. Feely et al. 2004).

Historically, pH has not been a common measurement on oceanographic cruises. pH probes are notoriously hard to keep calibrated, and the temperature and pressure of the same sample must be recorded during pH measurement. (At a constant pCO_2, higher temperatures and greater pressures decrease pH (Cao et al. 2007; calculations with van Heuven et al. 2009)). Also,

four different pH scales are commonly in use; older measurements did not always report which scale was used. Thus, pH has typically been derived from other carbonate chemistry parameters. However, measuring pH directly is preferable for accuracy, availability of associated error, and reproducibility. Direct measurements can be made spectrophotometrically, with a semi-permeable glass membrane, ion-sensitive field effect transistor (ISFET), or other kinds of measurements with a pH probe.

On the opposite end of the acidity spectrum is total alkalinity (TA): a solution's capacity to neutralize acid.

$$TA = OH^- + HCO_3^- + 2*CO_3^{-2} + B(OH)_4^- + NO_3^- + NO_2^- \ldots$$

Along with pH and TA, the other two major parameters of the carbonate chemistry system are dissolved inorganic carbon (DIC) and the partial pressure of carbon dioxide dissolved in the solution (pCO_2).

$$DIC = [CO_2(aq)] + [H_2CO_3] + [HCO_3^-] + [CO_3^{-2}]$$

When any two of the four carbonate chemistry characteristics (pH, pCO_2, DIC, TA) are known, the other two can be calculated.

Gaseous oxygen and carbon dioxide are conjugate species for oxygen molecules in marine photosynthesis and respiration.

<u>Photosynthesis</u> $CO_2 + H_2O + sunlight\ energy \rightarrow H_2CO + O_2$

<u>Respiration</u> $O_2 + H_2CO \rightarrow CO_2 + H_2O + chemical\ energy$

In marine settings, the carbon released in respiration may be in a number of chemical forms.

A final important chemical parameter (especially when considering how ocean acidification may affect coral reefs) is the carbonate saturation state, defined as

$$\Omega_{carb} = ([Ca^{-2}]\ [CO_3^{-2}]) / k_{carb}$$

where Ω_{carb} is the saturation state of a given carbonate mineral (aragonite or calcite) and k_{carb} is that mineral's solubility constant. When $\Omega < 1$, the solution is undersaturated; when $\Omega > 1$, the solution is supersaturated. Carbonate minerals dissolve readily in undersaturated solutions, and calcification occurs more easily the more supersaturated the solution. Optimal growing conditions is generally held to be $\Omega_{arag} \geq 3$ for scleractinan corals (e.g. Gattuso et al. 1998). High-magnesium calcite (HMC) is the most soluble carbonate mineral; low-magnesium (LMC) calcite is the least soluble; aragonite, the mineral most commonly found in coral skeletons, has a solubility in between that of the calcite varieties.

4 INSTRUMENTATION AND METHODS

To deploy sensors to make time-series measurements of environmental parameters at the EFGB reef crest, we designed and fabricated a custom stand for the sensors (Fig. 3). Its design accommodated several needs: secure sensor attachment, appropriate sensor orientation, ease for scuba divers to manipulate, the positioning of sensors among coral community, and minimal profile/environmental disturbance. A rectangular frame, comprised of welded stainless steel strut channel, had four faces to which a variety of sizes of PVC brackets could be attached at multiple levels. This arrangement provided a large degree of flexibility in the number, size, and orientation of devices that can be deployed, and it offered ease of attachment and access for each device. The brackets incorporated custom designed pins that divers can easily place, secure and remove underwater using simple locknuts and zip-ties. Used in conjunction with underwater-mateable cables, a modular approach to the deployment and maintenance of an ocean monitoring system is possible. The frame was supported by a central PVC tube, the length of which can easily be cut to achieve any suitable height. A stainless steel plate with milled slots to attach anchor bolts was originally made to anchor the frame to the seafloor; however, based on seafloor conditions at the sensor deployment site, the design was modified to firmly mount the stand to a railroad wheel that had been previously placed on the seafloor.

High-quality commercially available instruments were utilized to measure environmental parameters, provide electrical power, and store/transmit data. Fig. 3 shows these instruments deployed on the seafloor stand at the reef crest. A Seabird 16*plus* V2 CTD (SBE16) measured salinity, temperature, and pressure; it also powered and collected data from Wet-Labs bio-wiper equipped PAR, FLCD, and FLNTUS sensors measuring photosynthetically active radiation (PAR), chromophoric dissolved organic matter (CDOM), and turbidity/chlorophyll, respectively.

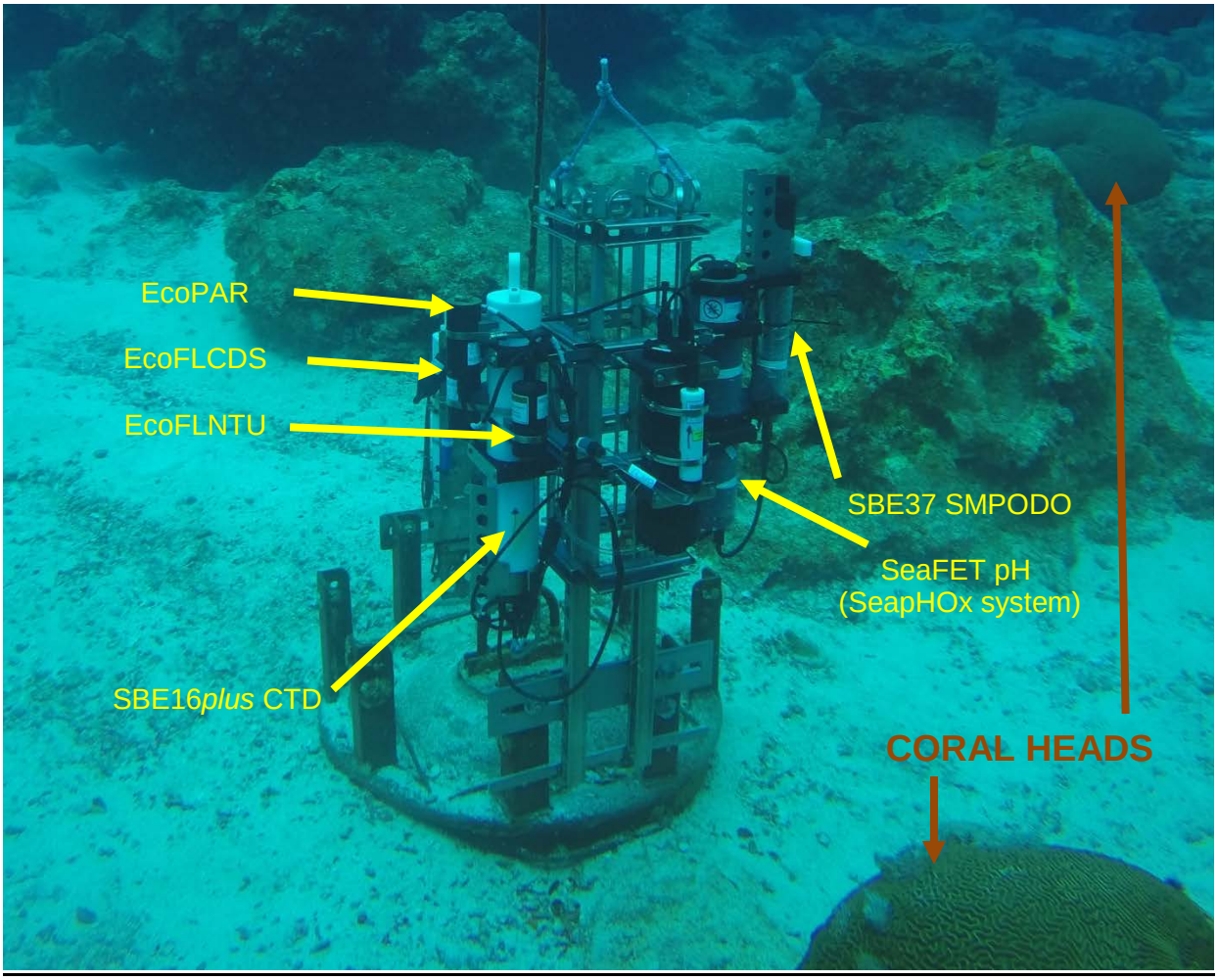

Fig. 3 Ocean acidification sentinel site framework with sensors deployed at EFGB. This custom designed and built framework is designed to minimize the sensor footprint on the reef, securely hold sensors in proper orientation, ensure all sensors measure water with the same properties, and facilitate sensor deployment and maintenance by SCUBA divers. A pair of healthy corals in the vicinity are marked. Photo credit: Michelle Johnston, NOAA.

A SeaFET potentiometric unit with two electrodes monitored seawater pH (Martz et al. 2010). The internal pH cell consists of an ISFET as the working electrode and an Ag/AgCl electrode bathed in a saturated KCl solution/gel as the internal reference electrode (the downside of using this electrode is that its reading includes an unknowable liquid junction potential across the frit separating it from the seawater). The external pH cell also consists of the ISFET as the working electrode, and its signal reflects a combination of both the H^+ and chloride species. Attached to the SeaFET is a Seabird 37-SMPODO CTD equipped with a pump; together the SeaFET and Seabird 37 form a SeapHOx unit. The Seabird 37 measures conductivity, temperature and the concentration of dissolved oxygen of water that first passes over the SeaFET's potentiometers.

During cruises to the EFGB on the NOAA ship *RV Manta*, the sensors were activated and then deployed on May 7, 2017 and recovered on July 6, 2017 by divers at EFGB (27.90902 N, 93.59755 W; Fig. 2b). The instruments were located at a depth of twenty-two meters, and less than half a meter above the reef crest at the same height as numerous coral colonies within 10 m (visible in Fig. 3). Measurements with each device were made at two hour intervals on the even integers starting at 10AM (i.e. 10AM, 12PM, 2PM, etc). In addition to the *in situ* measurements, discrete water samples were taken by divers at depth at the sensor site during deployment (May 8 at 11 AM) and recovery (July 6 at 1 PM) of the sensors and transported to laboratories at Texas A&M University for analysis of nutrient concentrations, conductivity, total inorganic CO_2, and TA. These laboratory derived carbonate chemistry parameters were used with the CO2SYS program (Pierrot et al. 2006) to calculate the Ω_{arag} and pCO_2 at the start and finish of the study period at the EFGB reef cap.

The chemical compositions of the discrete water samples were analyzed at Texas A&M University. Nutrient concentrations and conductivities were measured using an Astoria-Pacific

Analyzer and a Guildline Autosal, respectively, at the Geochemical and Environmental Research Group following standard procedures. Based on replicate analyses of standards, estimated precisions are of ± 1% NO_3^-, ± 2.5% $HPO_4^=$, ± 7.2% $HSiO_3^{-1}$, ± 11% NH_4^+, ± 4% NO_2^-, and ± 38% urea and ± 0.001 psu salinity. DIC and TA were measured using a VINDTA in the laboratory of K. Shamberger following standard methods, with estimated precisions of ±3 µmol kg^{-1} and ±1.5 µmol kg^{-1} or better for DIC and TA, respectively (e.g., Shamberger et al. 2017). Table 1 contains all results from the analyses of these discrete samples.

The instruments in the seafloor sensor package reported data as hexadecimal code, so upon recovery of the sensor package it was converted to readable ASCII characters. This conversion was accomplished using SBEDataProcessing software provided by Sea-Bird with the SBE16 and SeaFETCom software provided by Satlantic with the SeapHOx.

The instruments were deployed during the 59 Julian Day (JD) period from May 7, 2017 (JD 128) to July 6, 2017 (JD 187). Given the programmed data collection schedule, it was anticipated that 714 data points would be collected by each sensor; however, data was not collected during the entirety of the deployment period. The SBE16 collected data with its temperature, salinity, and pressure sensors and the attached Wet-Labs PAR, FLCD and FLNTUS sensors during the first 53 days of the deployment period, but it lost battery power early on JD 181 so it was unable to make measurements during the final 6.5 days of the deployment period. Also, due to a firmware mismatch, the SeapHOx CTD did not record 35 temperature and salinity readings. This issue occurred at irregular time intervals (never more than two in a row) that comprised about 4.9 % of the total potential SeapHOx CTD dataset. Because these readings were necessary to calculate pH values, these gaps are replicated in the pH dataset.

Table 1 Measured properties of discrete water samples

Parameter	**May 8, 2017**	**July 6, 2017**
Time of Day	11AM	1PM
NO_3^- (umol L^{-1})	0.23 ± 0.24	2.83 ± 0.79
$HPO_4^=$ (umol L^{-1})	0.55 ± 0.12	0.49 ± 0.08
$HSIO_3^-$ (umol L^{-1})	1.8 ± 0.08	3.39 ± 0.58
NH_4^+ (umol L^{-1})	0	1.04 ± 0.63
NO_2^- (umol L^{-1})	0.13 ± 0.01	0.19 ± 0.05
Urea (umol L^{-1})	0	0.48 ± 0.33
$NO_3^- + NO_2^-$ (umol L^{-1})	0.36 ± 0.25	3.03 ± 0.82
Number of samples	4	4
Salinity (psu)	36.3725 ± 0.001	35.1704 ± 0.005
Number of samples	4	3
TA (umol kg^{-1})	2399.3 ± 2.5	2376.3 ± 3.2
DIC (umol kg^{-1})	2066.4 ± 1.6	2058.7 ± 1.5
Number of samples	3	3
DIC/TA	0.86	0.87

Note: reported values are the average of the values obtained from all samples, and errors are standard deviations of N analyses of samples.

5 RESULTS

The first step in considering the results obtained from the instruments is to assess the quality of the basic temperature and salinity data by comparing values measured independently by the SBE16 and the SeapHOx. Fig. 4 shows no significant or consistent differences between values from the two sensors. Also, the *in situ* salinity measurements closely match values obtained from water samples in the laboratory (the latter are reported in Table 1). Water samples collected on May 8 have an average salinity of 36.373 ± 0.001 psu whereas the SBE16 reported 36.368 and 36.366 psu at 10 AM and 12 PM, respectively, times that are ± 1 hour of when water sample was collected (no corresponding values were available from the SeapHOx). The difference between values is at most 0.007. Water samples collected on July 6 at 1 PM have average have an average measured salinity of 35.170 ± 0.005 psu and the final SeapHOx salinity reading (10AM, 3 hours earlier) was 35.159 psu (no corresponding values were available from the SBE16). The difference between values is 0.011. Given the close agreement of all these values, we have confidence in the accuracy and precision of the autonomously recorded data.

However, there are times of increased variability between the sets of sensors. Times of increased difference between salinometer readings correlate with increased variability between thermometer measurements (Fig. 4: e.g. yellow zone), but there are also times when this is not the case: the cyan zone shows salinity, not temperature variability and the period of JD 159 – 167 shows temperature, not salinity variability. With the exception of the latter, all correlate with step changes in the site's salinity (Fig. 5). Increased variability of these standard physical parameters for up to a day may indicate the passage of a marine or meteorological front. Local wind gusts can account for some of these step changes, but there is no tight correlation between wind speed and salinity (Fig. 6). For example, around JD 170 Tropical Storm Cindy caused a rapid salinity

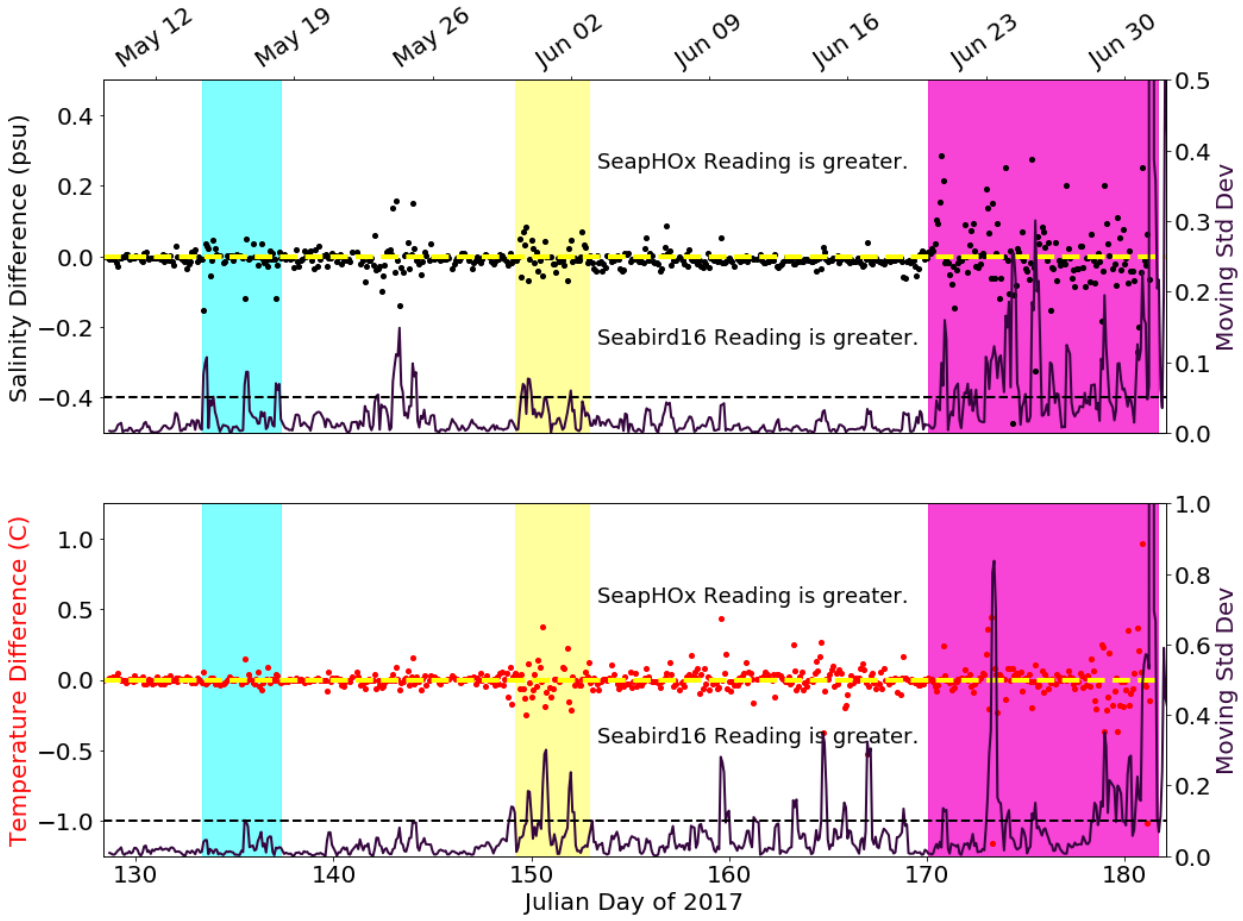

Fig. 4 A comparison of SBE16plus V2 and SeapHOx measurements to assess data quality. Time-spans when greater differences of just salinity, just temperature, or both salinity and temperature measurements occur are highlighted by the colors cyan, yellow, and green, respectively. During JD 153 – 159, the differences of salinity and temperature seem to be slightly greater than at other periods of low variability, but differences remain under the apparent threshold values (dashed lines) of 0.05 for salinity and 0.1 for temperature for the three-point moving standard deviation (solid line; right y-axis).

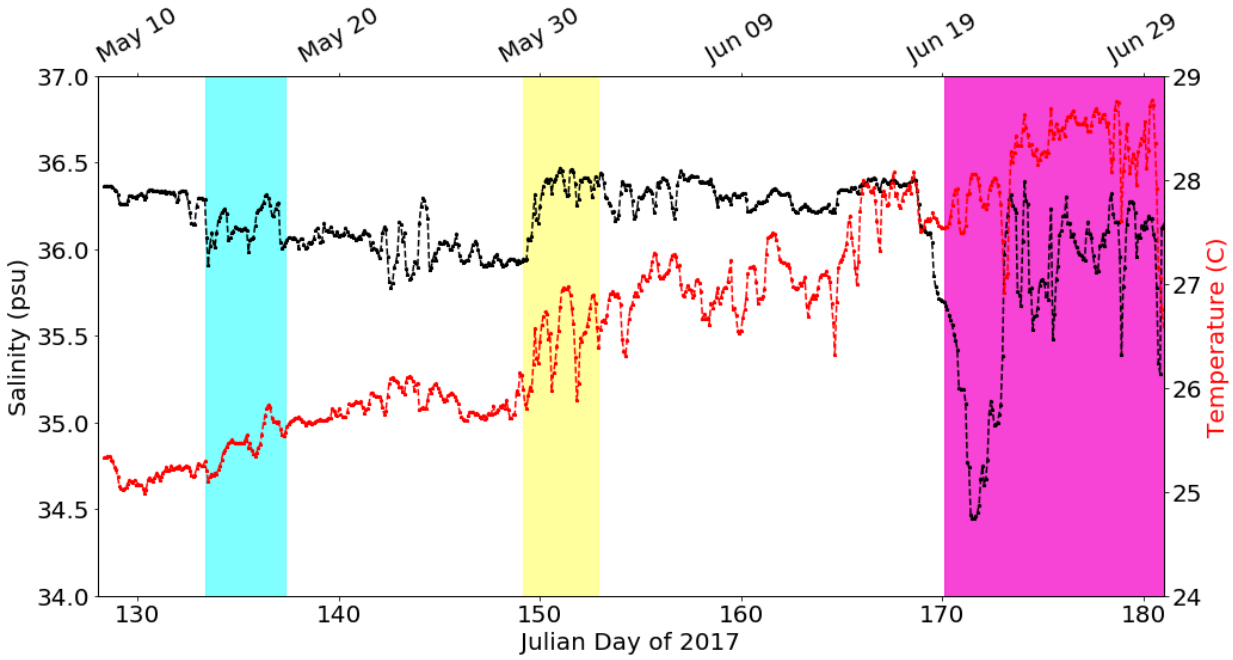

Fig. 5 Zones of increased sensor variability mapped against salinity and temperature. Zones are replicated from Fig. 4, and data is from the SBE16*plus* sensors. In the cyan zone, salinity undergoes a step-change from 36.4 to 36.1; yellow denotes a step-change from 35.9 to 36.4 psu; pink shows the dramatic freshening from Tropical Storm Cindy, following which the salinity never becomes as stable as seen earlier in the record.

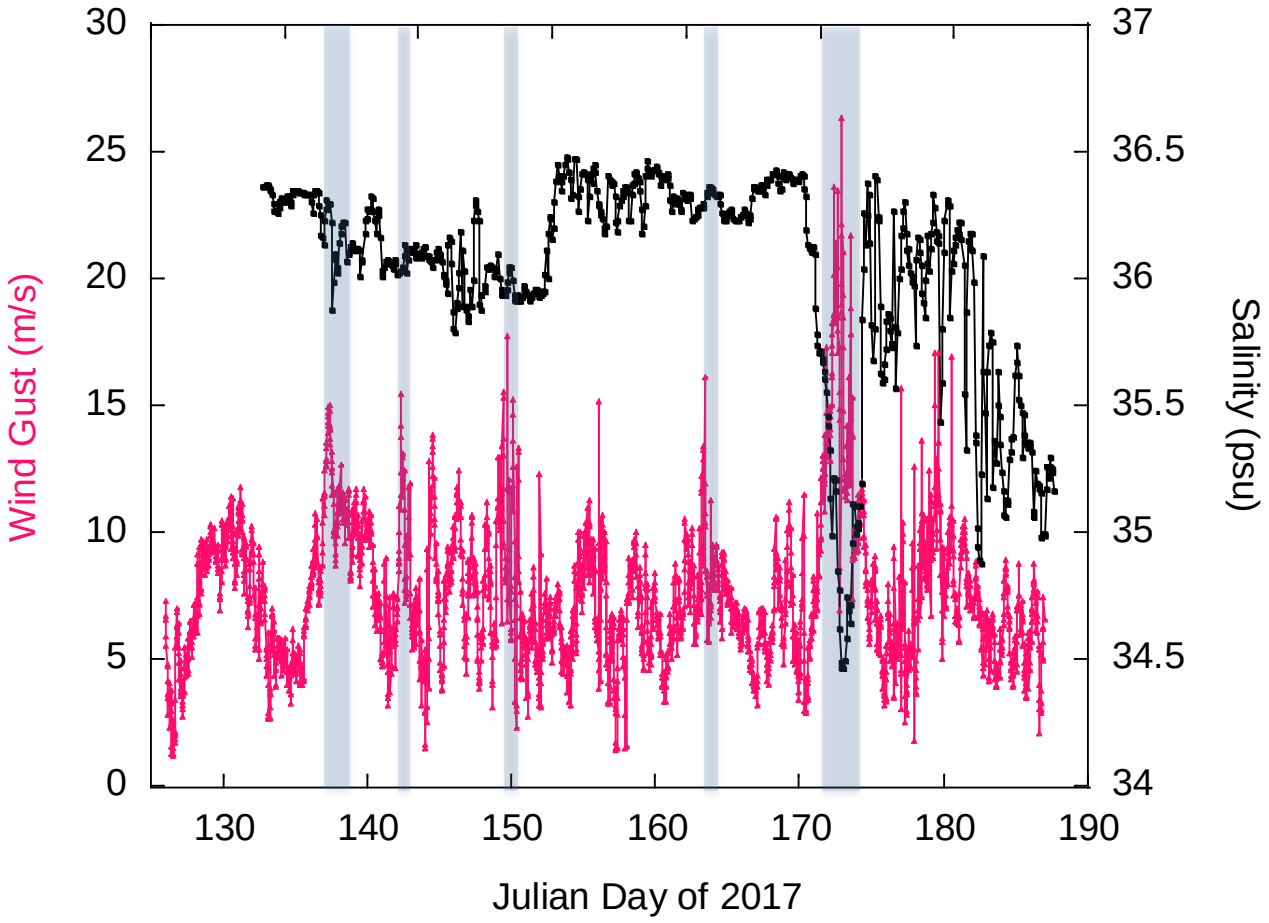

Fig. 6 Windiness correlates with spikes of salinity. Blue highlighted zones mark co-temporal salinity (SeapHOx; black) and wind gust (Buoy V; pink) increases, all occurring when wind gusts exceed 15 m/s. Wind gust data publically available at http://tabs.gerg.tamu.edu/.

decrease of ~2 psu, leading to substantial, prolonged variability in both temperature and salinity (Fig. 4). Thus, all sensors appear to accurately record their aliquots, with variability during periods of water mass interaction reflecting true variability of water properties.

Having established the quality of data via comparison of independent measurements, we now look to the overall seasonal changes in water properties and their influence on carbonate chemistry. These changes can be determined two ways: by averaging 24 hours of data to get representative start- and end-member figures (summarized in Table 2) and by applying linear regressions to characterize overall trends. The first method yields a temperature increase of 3.27 C (SeapHOx); the second method yields increases of 3.72 C (SBE16; R = 0.915) and 3.95 C (SeapHOx; R = 0.958) (Fig. 7). A slightly smaller change is obtained from the difference between start- and end-values because cooling caused by Cindy, an event that lasted only a few days, resulting in the last data points falling well below both fitted trendlines in Fig. 7. To avoid undue influence of Cindy, the values from the linear regression is used for assessing seasonal changes in environmental conditions, which are characteristic of this location during the transition from spring to summer.

The two methods yield similar values of the overall change of pH change during the study period. The first method shows pH external decreasing by 0.039 on the total scale and pH internal decreasing by 0.056, changes almost obscured by the propagated error. Using linear regressions produces similar pH decreases over the deployment of 0.047 (R = -0.432; pH-ext) or 0.041 (R = -0.566; pH-int) units on the total scale. A trend of decreasing pH is present in each of these values, but the smaller R values produce less certainty than temperature's regressions' values. The other carbonate chemistry parameters are analyzed with only the start- and end-member method, using values from the discrete water samples (see Table 2). Measured values of

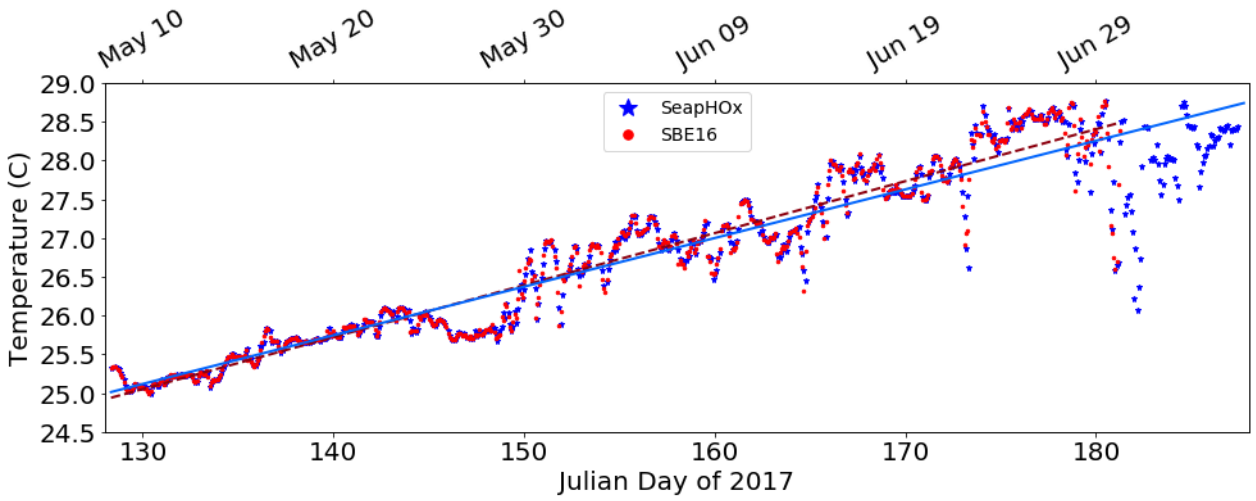

Fig. 7 A comparison of SBE16plus and SeapHOx temperature data with linear regressions. SeapHOx (blue stars, solid line; temperature = 0.0627 C d^{-1} * Julian Day + 16.963 C; R^2 = 0.918) and SBE16 (red dots, dashed line, temperature = 0.0671 C d^{-1} * Julian Day + 16.334 C; R^2 = 0.837) data exhibit linear relationships with high correlation coefficients and similar slopes. During the 59 day study period, the regressions record increases of 3.95 C (SeapHOx) and 3.72 C (SBE16).

Table 2 Late spring and mid-summer chemical characteristics of study site

Parameter	**Start**	**End**	**Change**	**Start**	**End**	**Change**
Day	May 1, '15	Aug 28, '15	120 days	May 9, '17	July 5, '17	60 days
Temp (C)	24.12	29.32	5.2±0.34	25.08±0.04[a]	28.35±0.08[a]	3.27±0.09
Salinity (psu)	36.22	36.24	0.02±0.08*	36.29±0.02[a]	35.13±0.10[a]	-0.96±0.1
DIC (umol kg^{-1})[b]	2019±7.4	2081±7.6	65.5±10.66	2066.6±1.6	2058.7±1.5	-7.9±2.2*
nDIC	1950.	2010.	60.	1989.28	2049.29	60.±2.14
TA[b] (umol kg^{-1})[b]	2390.5±2.7	2401.2±5.7	10.6±6.3*	2399.3±2.46	2376.3±3.2	-23.0±4.0
nTA	2414.1±2.6	2400.6±7.4	-12.65±7.4*	2309.6	2365.5	55.9±4.0
pCO_2 (ppm)[c]	388.6	457.9	69 ± 29	392.2	450.1	57.9
pH[c]	8.166[b]	7.975[b]	-0.191	8.061±0.005[a]	8.009±0.003[a]	-0.052±0.006*
Ω_{arag}[c]	3.69 ±0.11	3.87±0.12	0.18 ± 0.16*	3.72	3.68	-0.04*
N	7	13		12	12	

***** Essentially no change.

[a] Reported 2017 temperature, salinity, and pH values are averages and standard deviations of the earliest and latest full diurnal cycles of this study from SeapHOx instruments. Reported errors are propagated standard deviations.

[b] Laboratory results.

[c] Calculated from with CO2SYS from laboratory results of DIC and nTA.

Reported 2015 start and end values are from a TAMU cruise and a NOAA OAP cruise respectively.

DIC and TA in samples collected at the start and end of the study both decreased slightly: 7.9 umol kg^{-1} and 23.0 umol kg^{-1} respectively. Values of pH, Ω_{arag} and pCO_2, calculated from DIC and TA using CO2SYS, decreased by 0.05 units and 0.04 units and rose by 57.9 ppm, respectively. This seasonal behavior matches that of sites at similar latitude (see Discussion).

On the seasonal timescale as well as a finer temporal resolution, we observe overall correlations between important parameters. The timing of the parameters' cycles is crucial to understanding how they relate to and affect one another. For each set of parameters measured, a linear relationship was established and its correlation coefficient calculated between the raw data (each point being determined by the contemporaneous values of two parameters; e.g. Fig. 8). Then the second parameter is lagged by two hours, and a new correlation coefficient is calculated, i.e. the last point of the first parameter and first point of the second parameter are removed so that the first parameter's values would be matched with the value measured two hours later of the latter. This process is repeated up to 60 hours (e.g. Fig. 9), and the greatest correlation coefficient of that pair of parameters is listed as an R value in Table 3 with the lag when it occurred. Each iteration removes a point from the correlation: the sample size starts as 636 and shrinks to 606 (95.3%) for the longest lags. Thus, long lags become progressively less useful; lags greater than 24 hr are corrected modulo 24 and mentioned only so far as they cyclically agree with shorter lags. Significant correlations (denoted by boldface) are held to be those that are both lag less than 24hr and are ≥ 0.315 (which corresponds to an R^2 value of 0.1).

The highest calculated R values are for the sets of SeapHOx and SBE16 thermometers (R = 0.996) and salinometers (R = 0.988) and occur at 0 lag. This result is a strong indication that, as considered at the beginning of this section, both systems are reporting reproducible values at the same time.

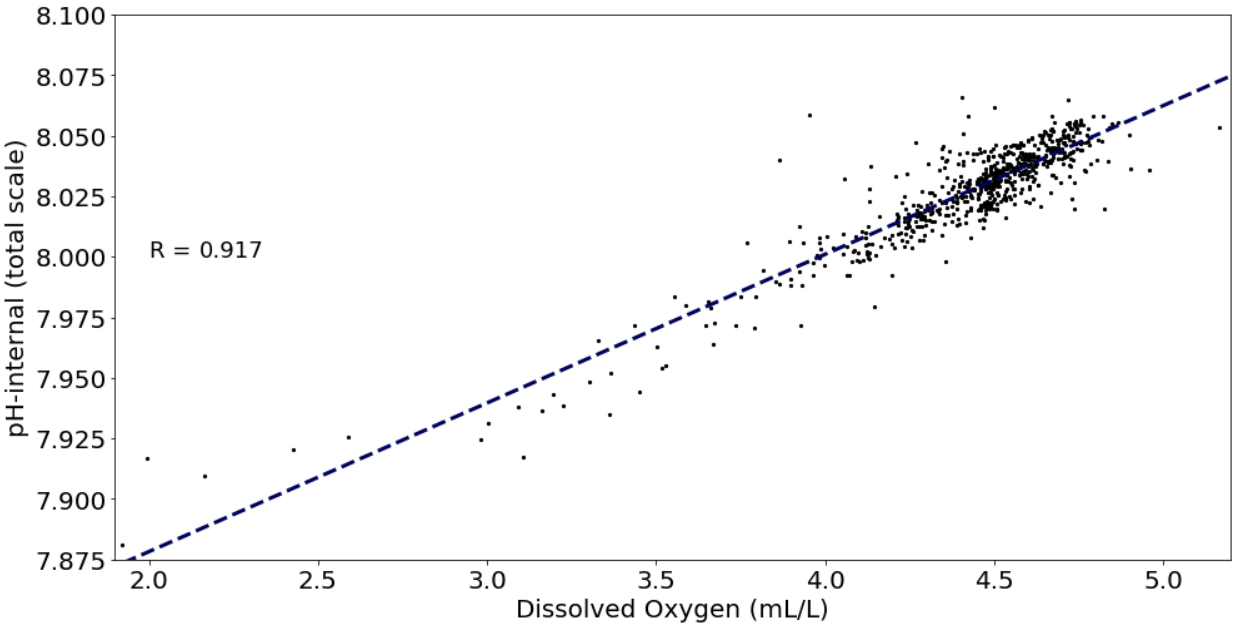

Fig. 8 The relationship between pH-internal and DO exhibits a high degree of linearity. Dashed blue line is best fit (pH = 0.06137 * DO + 7.7555).

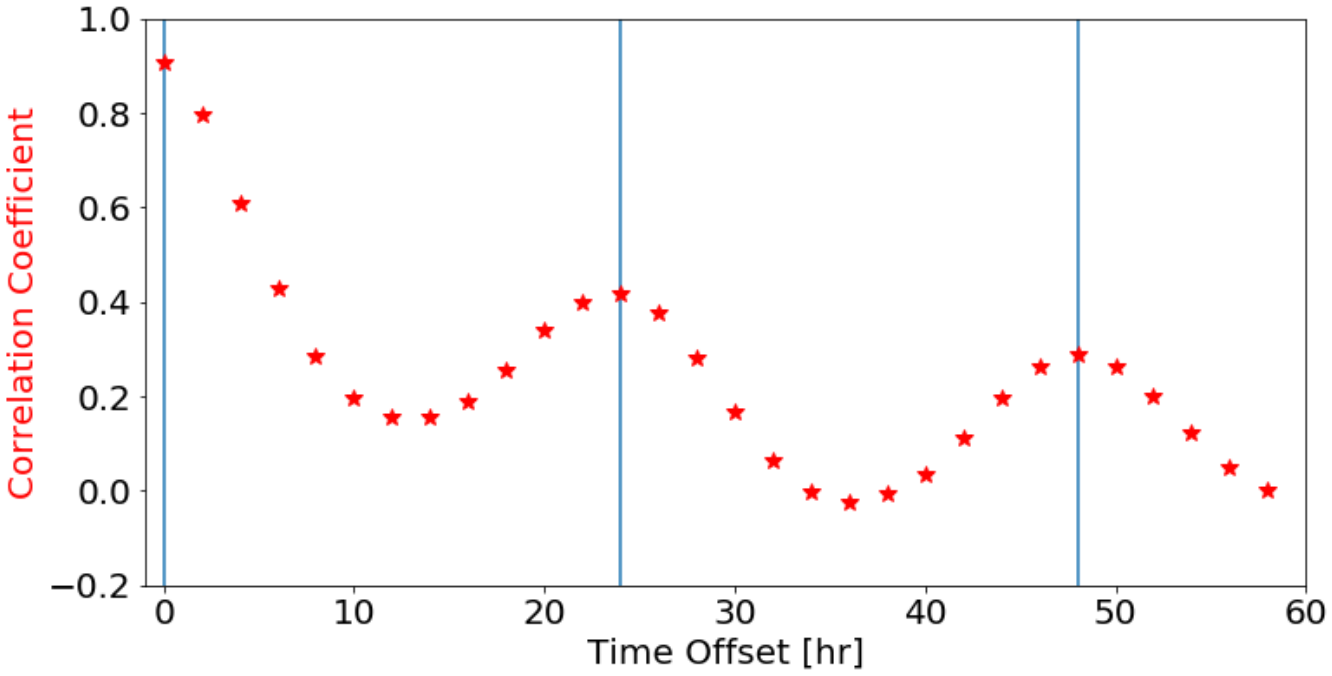

Fig. 9 pH (internal) and DO are well correlated. DO is the first parameter, and pH (presumed to be dependent) is the second, i.e. the parameter that gets lagged. Blue lines indicate lags of 0, 24, and 28 hours. Maximum R = 0.905 occurs at lag of 0 hours.

Table 3 Correlations between parameters for entire study period

	SeapHOx temp	SeapHOx salinity	pH-internal	pH-external	DO	SBE16 temp	SBE16 salinity	SBE16 pressure	Chl-a Fluores	Turbidity	CDOM Fluor	PAR
SeapHOx temp	–	-0.274	**-0.532**	**-0.366**	-0.358	**0.996**	-0.285	-0.164	0.319	0.158	-0.110	-0.063
	–	*58 (10)*	***6***	***8***	*32 (8)*	***0***	*58 (10)*	*0*	*48 (0)*	*48 (0)*	*48 (0)*	*12*
SeapHOx salinity	-0.221	–	0.539	0.587	0.463	-0.221	**0.988**	0.118	-0.184	-0.281	0.045	0.122
	6	–	*38 (14)*	*38 (14)*	*38 (14)*	*6*	***0***	*0*	*2*	*2*	*58 (10)*	*18*
pH-internal	-0.535	-0.305	–	**0.910**	**0.906**	-0.537	0.302	0.300	-0.176	-0.118	0.077	**0.322**
	40 (16)	*2*	–	***0***	***0***	*40 (16)*	*0*	*56 (8)*	*16*	*22*	*42 (18)*	***2***
pH-external	-0.387	**0.405**	**0.910**	–	**0.823**	-0.387	**0.405**	0.259	-0.077	-0.155	0.032	**0.316**
	58 (10)	***0***	**0**	–	***0***	*58 (10)*	***0***	*56 (8)*	*14*	*22*	*0*	***2***
DO	**-0.329**	0.155	**0.906**	**0.823**	–	-0.330	0.164	0.356	-0.110	-0.089	0.055	**0.385**
	0	*4*	***0***	***0***	–	*40 (16)*	*4*	*56 (8)*	*16*	*22*	*42 (18)*	***4***
SBE16 temp	**0.995**	-0.276	**-0.531**	**-0.366**	-0.358	–	-0.285	-0.167	0.316	0.155	-0.110	-0.063
	0	*58 (10)*	***6***	***6***	*30 (6)*	–	*58 (10)*	*0*	*48 (0)*	*48 (0)*	*46 (22)*	*12*
SBE16 salinity	-0.228	**0.988**	0.545	0.587	0.465	-0.230	–	0.110	-0.184	-0.285	0.045	0.114
	4	***0***	*38 (14)*	*38 (14)*	*38 (14)*	*50 (2)*	–	*0*	*2*	*0*	*58 (10)*	*16*
SBE16 pressure	-0.179	0.155	0.292	0.255	**0.954**	-0.270	0.148	–	-0.237	0.170	0.055	-0.560
	48 (0)	*24 (0)*	*16*	*16*	***18***	*0*	*24 (0)*	–	*8*	*0*	*16*	*32 (8)*
Chl-a Fluores	0.270	-0.195	-0.311	-0.205	-0.318	0.270	-0.200	0.207	–	**0.642**	-0.071	-0.100
	0	*14*	*42 (18)*	*42 (18)*	*40 (16)*	*0*	*16*	*0*	–	***0***	*2*	*12*
Turbidity	0.095	-0.285	-0.268	-0.253	-0.872	0.095	-0.286	0.170	**0.642**	–	0.032	0.055
	58 (10)	*4*	*42 (18)*	*42 (18)*	*40 (16)*	*58 (10)*	*6*	*0*	***0***	–	*20*	*44 (20)*
CDOM Fluor	-0.253	0.071	0.192	0.134	0.100	-0.256	0.071	0.100	-0.114	-0.126	–	0.110
	58 (10)	*48 (0)*	*58 (10)*	*58 (10)*	*58 (10)*	*58 (10)*	*52 (4)*	*42 (18)*	*50 (2)*		–	*32 (8)*
PAR	-0.063	0.164	**0.330**	**0.315**	**0.399**	-0.063	0.155	-0.568	-0.105	0.055	0.071	–
	36 (12)	*6*	***20***	***20***	***20***	*38 (14)*	*6*	*40 (16)*	*12*	*52 (4)*	*2*	–

Listed are the maximum R values for lead-lag correlations with the lag (in hours) of the horizontal label relative to the vertical label. When the maximum R value occurred after 24 hours, its lag is reduced modulo 24 and placed in parentheses. Correlations greater than or equal to 0.315 AND at a time lag < 24 hours are bolded.

The low R values of PAR indicate that it does not correlate well with most other parameters, though we expect its direct effects on temperature and Chl-a fluorescence to produce a statistical link. One reason may be because PAR's value is not truly cyclic: its value is essentially zero during many hours each night (totaling about 51% of the study period). Irregularities due to cloud cover, sea surface roughness would affect both daily PAR and temperature values, but a decoupling of their correlativity (R = -0.063 at 12 hours) could be due to the high heat capacity of seawater (causing a delay in peak temperature and a broader curve of its values). PAR's best correlation comes with pressure. Although these parameters are driven by the effects of different celestial bodies (solar insolation and lunar tides), their correlation coefficients have a regular 12 hour cycle peaking at -0.564. The R values between PAR and both DO and pH are significant, especially as concerns relative timing; this will be discussed in greater detail in the Discussion. Aspects of Chl-a behavior deserve closer analysis as to why its cross-correlation with PAR is so low (R = -0.105 at 12 hour lag), even though we usually see a tight relationship in graphical representations (Figs. 12 – 16).

Like PAR, Chl-a has very low correlation coefficients with other parameters: it correlates with temperature (R = 0.316) but only at a lag of 48 hours. Fig. 10 shows that temperature and Chl-a do not correlate; the steady decrease is indicative of parameters whose best correlation occurs at a lag of zero, but this value is an insignificant 0.270. This method simply does not give helpful information in understanding this relationship. The reason for the low utility may be caused by the zero value of PAR for 10 hours each night, the anomalous behavior of the Chl-a signal during the first ~14 days of the study period (discussed in depth below), or the numerous complications in interpreting Chl-a fluorescence, including the possibility of inconsistent beam attenuation by particulates, variable Chl-a concentration within phytoplankton,

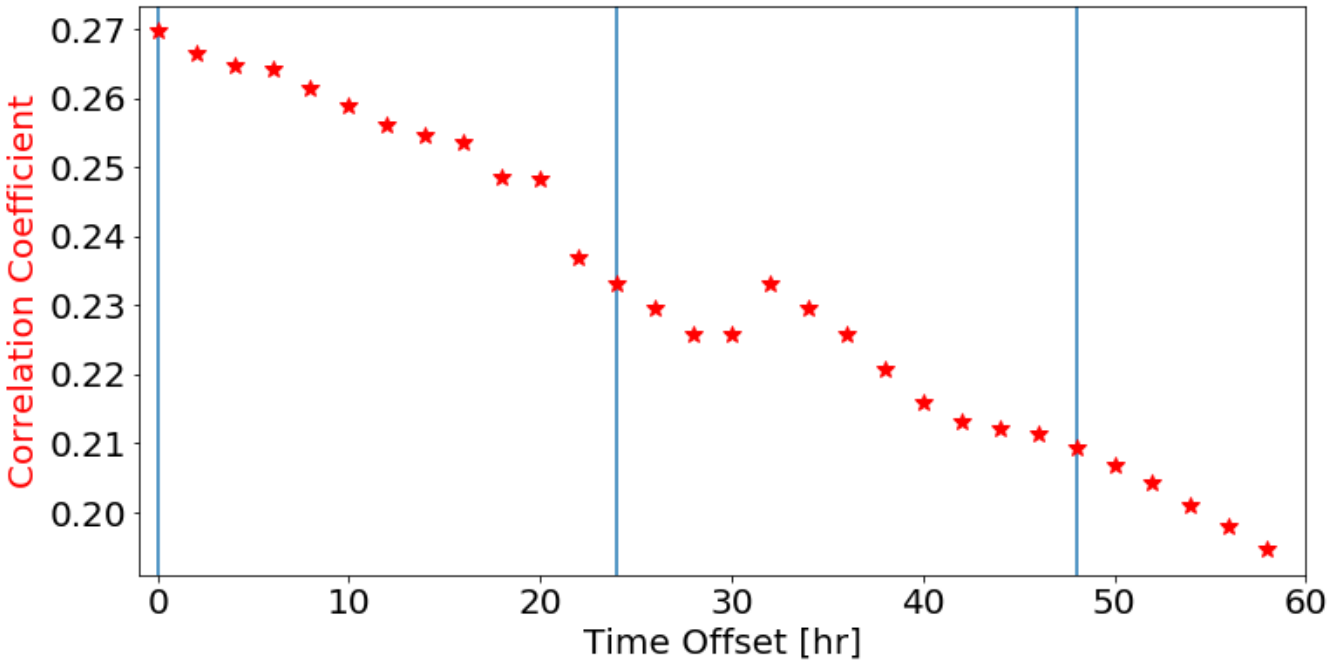

Fig. 10 Chl-a Fluorescence and temperature (SBE16) do not correlate. Temperature is the first parameter; Chl-a is the second, the parameter that gets lagged. Blue lines indicate lags of 0, 24, and 48 hours.

and a variable fluorescence yield of chlorophyll (Marra 1997). Another statistical tool is needed to show the cyclic behavior of Chl-a and link it to that of PAR.

In addition to overall links (or absence thereof) between parameters, clear variations in environmental conditions also occur on daily and weekly time scales. Step-changes in salinity (see Fig. 5) indicate possible water mass interactions and therefore potential shifts in parameter values that can degrade long-term correlations, necessitating analysis at finer timescales. To mitigate such effects, we concentrated on how each parameter changed on a daily basis during five week-long periods that occur at various parts of the study. These periods were selected by identifying time periods of regular water-mass behavior as indicated by salinity. As shown in Fig. 11, Weeks A and B start and end with a consistent, albeit different salinity and exhibit some internal variation; Weeks C and D are periods of relative stability before Tropical Storm Cindy; Week E, chosen to reflect water conditions post-Cindy, exhibits marked though consistent variability. Each 'day' is defined as 38 hours, with the exception of Week E whose days are 34 hours long because of the limits placed on the amount of available data by Cindy and by the end of the study period. This expanded day creates some overlap in the data (as each day starts 24 hours after the previous day started) but is necessary so that any cycles not centered at noon could be elucidated. The seven days of each week were compared to one another, and an average day's parameters were found by averaging for each parameter the values measured at midnight, 2AM, etc. separately (missing data points were excluded from calculations). Table 4 shows the results of these calculations. PAR, Chl-a, pressure, temperature, pH and DO showed regular patterns (i.e. daily cycles) during each week.

A major goal of this study is to characterize the typical behavior of environmental data at EFGB. Ideally, this baseline would be representative of chemical parameters' typical behavior

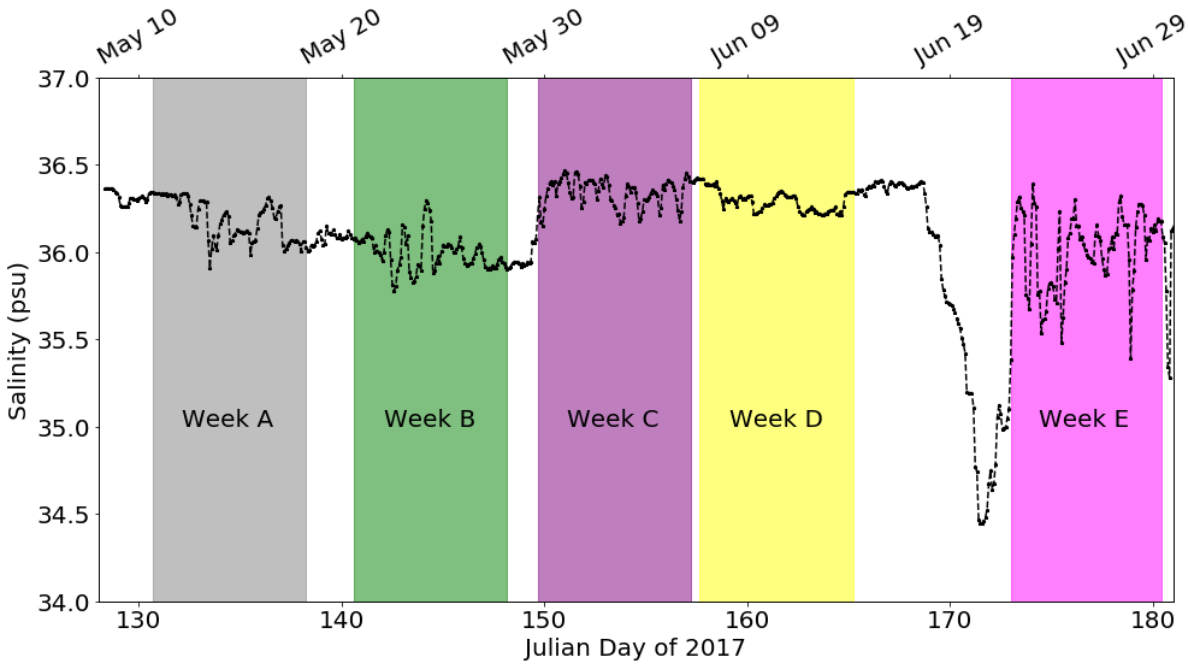

Fig. 11 Record of salinity with time intervals corresponding to Weeks A – E. Salinity data measured by the SBE16*plus* SeapHOx is shown; Weeks A – E are detailed in Table 4. Note that Cindy (fresher water starting circa JD 168) and the end of the study place limitations on the length and position of Week E.

Table 4 Weekly analysis of how parameters cycle daily

	Week A	**Week B**	**Week C**	**Week D**	**Week E**
First Day	May 11, 2017	May 21, 2017	May 30, 2017	June 8, 2017	June 22, 2017
Day of Week	Thursday	Sunday	Tuesday	Thursday	Thursday
Last Day	May 17, 2017	May 27, 2017	June 5, 2017	June 14, 2017	June 28, 2017
Day of Week	Wednesday	Saturday	Monday	Wednesday	Wednesday
Temp Avg Range[a]	**0.243**	**0.273**	**0.754**	**0.629**	**0.752**
SD[b] (RSD)[c]	0.075 (30%)	0.078 (29%)	0.214 (28%)	0.180 (29%)	0.203 (27 %)
HV[d] (RHV)[e]	0.19 (79%)	0.12 (43%)	0.31 (41%)	0.22 (35%)	0.27 (36%)
Mean	25.395	25.879	26.770	26.987	28.335
Max	25.843	26.110	27.293	27.491	28.754
Min (C)	25.098	25.689	25.878	26.315	26.918
Peak before PAR[f]	+2 hr	-4 hr	0 hr	0 hr	-4 hr
Sal Avg Range	**0.243**	**0.284**	**0.246**	**0.116**	**0.785**
SD (RSD)	0.0706 (29%)	0.0836 (29%)	0.073 (30%)	0.036 (31%)	0.211 (27%)
HV (RHV)	0.103 (43%)	0.0927 (33%)	0.0687 (28%)	0.052 (45%)	0.209 (27%)
Mean	36.188	36.000	36.3395	36.2915	35.991
Max	36.343	36.299	36.4703	36.422	36.394
Min (psu)	35.909	35.779	36.151	36.213	35.049
pH-int Avg Range[g]	**0.0354**	**0.0351**	**0.0299**	**0.0501**	**0.0518**
SD (RSD)	0.0097 (27%)	0.0093 (26%)	0.0076 (25%)	0.014 (29 %)	0.013 (26 %)
HV (RHV)	0.0072 (20%)	0.0089 (25%)	0.0080 (27%)	0.0094 (19%)	0.0105 (20%)
Mean	8.0426	8.0358	8.0356	8.0296	8.0160
Max	8.0646	8.0583	8.0659	8.0534	8.0315
Min (total scale)	8.0064	7.9885	7.9924	7.9794	7.9314
pH-ext Avg Range[g]	**0.0343**	**0.0368**	**0.0323**	**0.0507**	**0.0511**
SD (RSD)	0.0095 (28%)	0.0100 (27%)	0.0085 (26%)	0.015 (29%)	0.013 (26%)
HV (RHV)	0.0076 (22%)	0.0127 (35%)	0.0100 (31%)	0.0106 (21%)	0.0118 (23%)
Mean	8.0805	8.0831	8.095	8.0867	8.0626
Max	8.1113	8.1185	8.127	8.1133	8.0836
Min (total scale)	8.0504	8.0314	8.048	8.0333	7.9820
Peak before PAR	-2 hr	-2 hr	-2 hr	-2 hr	-2 hr
DO Avg Range	**0.61**	**0.56**	**0.48**	**0.91**	**0.83**
SD (RSD)	0.18 (30%)	0.15 (26%)	0.13 (27%)	0.25 (27%)	0.21 (26 %)
HV (RHV)	0.11 (17%)	0.10 (18%)	0.08 (17%)	0.13 (14%)	0.16 (19%)
Mean	4.52	4.54	4.49	4.46	4.32
Max	4.87	4.90	4.84	5.17	4.63
Min (mL L^{-1})	3.90	3.87	3.86	3.65	3.00
Peak before PAR	-2 hr	-2 hr	-2 hr	-2 hr	-2 hr
PAR Avg Range	**452**	**381**	**373**	**436**	**340**
SD (RSD)	133 (29%)	114 (30%)	111 (30%)	140 (32 %)	101 (30 %)
HV (RHV)	18 (3.9%)	37 (9.8%)	24 (6.5%)	16 (3.7%)	30 (8.8%)
Mean	108.3	87.2	87.9	118.8	77.6
Max	505.25	461	463	473	418
Min (mmol $m^{-2}s^{-1}$)	0.041	0.041	0.041	0.041	0.041
Time of Peak	12PM	12PM	12PM	12PM	12PM

Table 4 Weekly analysis of how parameters cycle daily (continued)

	Week A	Week B	Week C	Week D	Week E
Chl-a Avg Range	**0.336**	**0.528**	**0.568**	**0.633**	**0.336**
SD (RSD)	0.095 (28%)	0.166 (31%)	0.168 (30%)	0.182 (29%)	0.100 (30%)
HV (RHV)	0.258 (77%)	0.103 (19%)	0.085 (15%)	0.123 (19%)	0.052 (15%)
Mean	0.511	1.202	1.421	1.512	1.224
Max	1.310	1.713	1.957	2.284	1.579
Min (mg m^{-3})	0.105	0.933	1.104	1.237	1.093
Peak before PAR	-2 hr	-2 hr	0 hr	-2 hr	-2 hr
Press Avg Range	**0.5843**	**0.6443**	**0.433**	**0.5764**	**0.8**
SD (RSD)	0.180 (31%)	0.192 (30%)	0.122 (28%)	0.197 (34%)	0.254 (31%)
HV (RHV)	0.0749 (13%)	0.1269 (20%)	0.100 (23%)	0.071 (12%)	0.142 (18%)
Mean	21.737	21.7124	21.696	21.685	21.644
Max	22.118	22.1400	21.9860	21.987	22.207
Min (dbar)	21.441	21.202	21.276	21.36	21.130
CDOM Avg Range	**11.274**	**6.909**	**5.601**	**5.5427**	**6.1722**
SD (RSD)	3.409 (30%)	2.030 (29%)	1.73 (31%)	1.641 (30 %)	1.578 (26 %)
HV (RHV	3.63 (32%)	2.173 (31%)	1.73 (31%)	1.58 (28%)	1.653 (27%)
Mean	9.409	8.633	8.5925	8.4309	7.2820
Max	17.3096	13.7218	11.8156	14.1495	12.5549
Min (mg m^{-3})	-0.1871	3.4296	4.1762	4.1327	2.5816
Turb Avg Range	**0.073**	**0.149**	**0.042**	**0.361**	**0.204**
SD (RSD)	0.018 (24%)	0.033 (22%)	0.012 (28%)	0.081 (22%)	0.051 (25%)
HV (RHV)	0.016 (22%)	0.031 (21%)	0.011 (26%)	0.057 (16%)	0.051 (25%)
Mean	0.292	0.301	0.280	0.315	0.305
Max	0.405	0.621	0.336	2.345	0.772
Min (NTU)	0.274	0.262	0.247	0.249	0.255
"Length" of day	38hr:4pm-4am	38hr:2pm-2am	38hr:4pm-4am	38hr:4pm–4am	34hr:8pm-6am
'Cloudy' Days[h]	1	5 (2 > 390)	4	2	6 (1 > 390)
Days in week	7	7	7	7	7
N for std dev	19	19	19	19	17
Accompanying Fig.	12	13	14	15	16

[a] Avg Range ≡ average of the seven days' ranges.
[b] SD ≡ Avg Range's standard deviation.
[c] RSD ≡ SD divided by Avg Range.
[d] HV ≡ hourly variability. Average standard deviation of each hour's average; Each hour (e.g. 12pm) has a std dev expressing how conditions vary at that time throughout the week. HV is N (from the penultimate row of Table 4) standard deviations averaged together.
[e] RHV ≡ relative hourly variability. HV divided by Avg Range.
[f] Peak before PAR ≡ number of hours parameter's peak arrives before that of PAR. Positive numbers are before the PAR peak; negative numbers are after the PAR peak.
[g] pH sensitivities are reported to four decimal places so that a two digit RHV may be calculated. The pH meters have precisions better than 0.001, an initial accuracy of 0.05 and a stability of 0.05 $month^{-1}$.
[h] Cloudy day defined as PAR max < 400 mmol $m^{-2}s^{-1}$.
Notes: Temp, Salinity readings are from SBE16plusV2 instrument.
See Fig. 10 to position Weeks A-E within full salinity dataset. See Fig. 12 to see how average temperature increases over time.

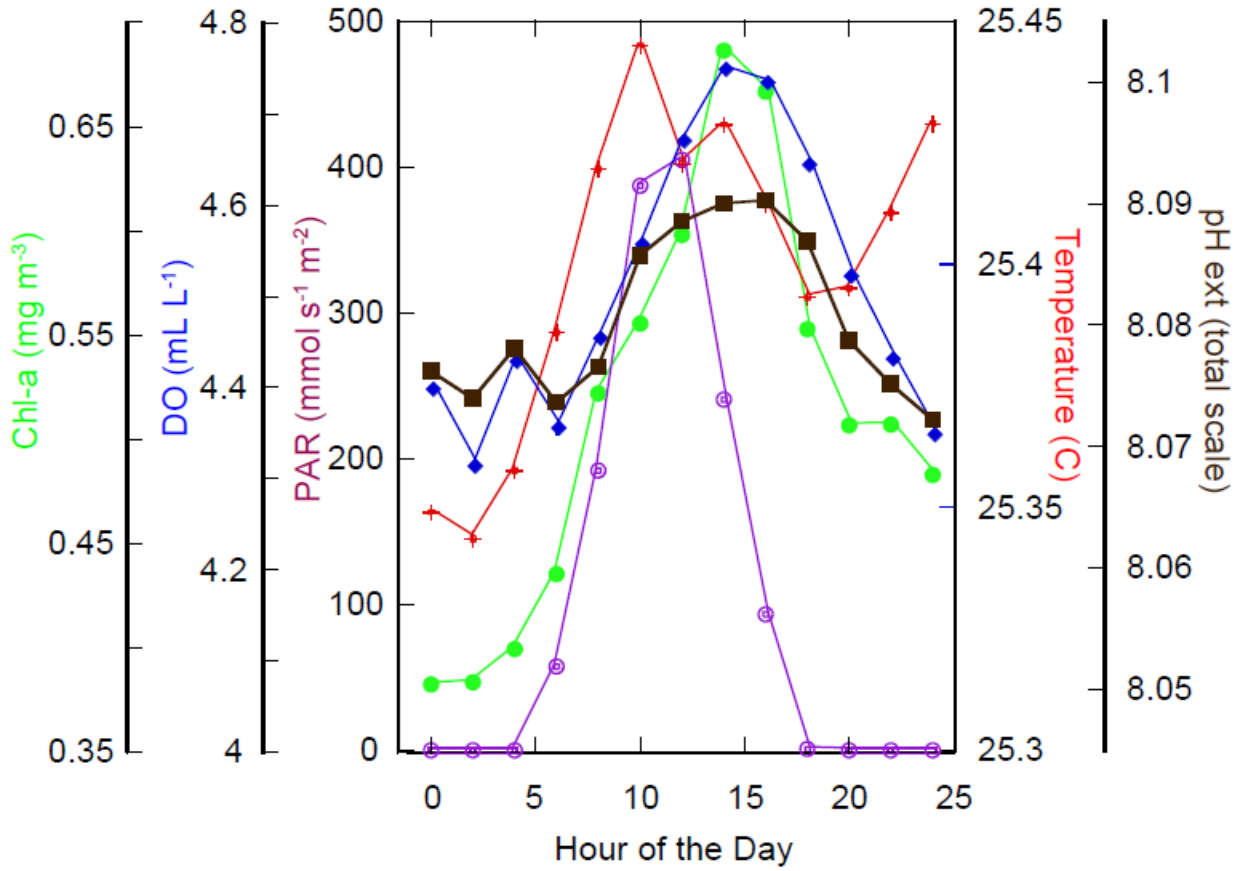

Fig. 12 The average values of select parameters over Week A (May 11-17) are shown. Note the strong correlation between DO (blue) and pH (brown). Temperature (red) peaks earliest at 10AM.

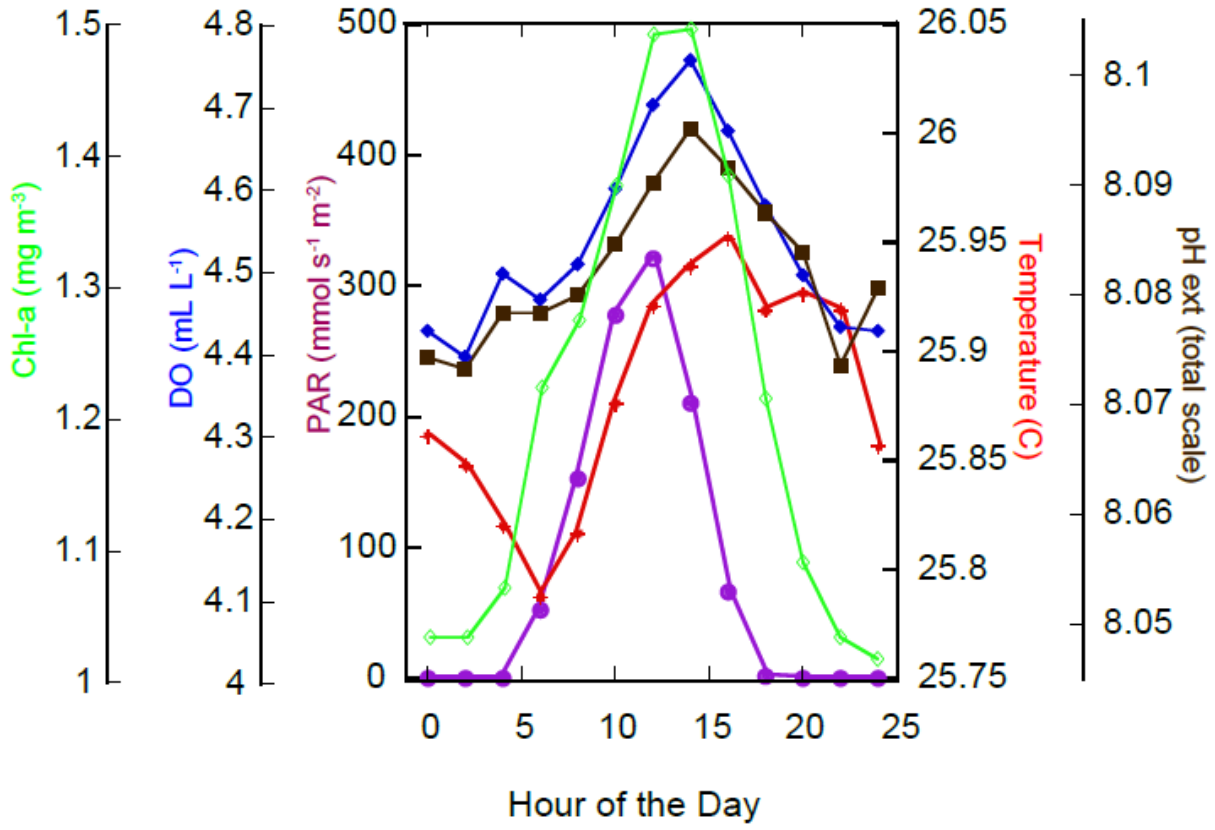

Fig. 13 The average values of select parameters over Week B (May 21-27) are shown. Note the strong correlation between DO (blue) and pH (brown). Temperature (red) peaks last at 16:00.

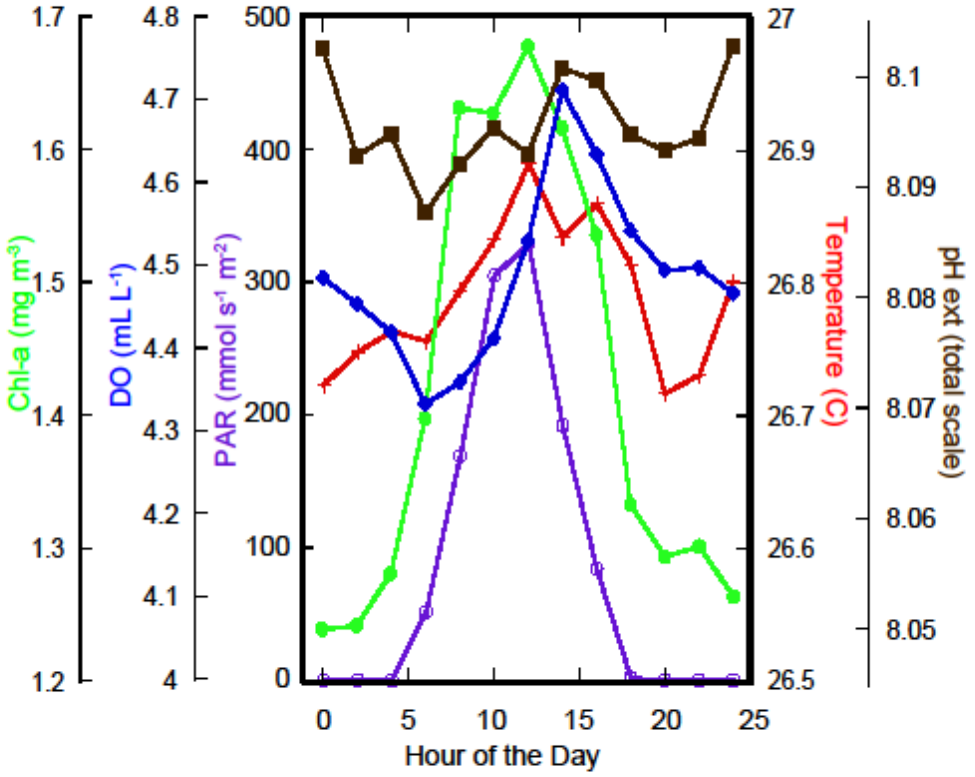

Fig. 14 The average values of select parameters over Week C (May 30 – June 5) are shown. This week shows the weakest correlation between DO (blue) and pH (brown). Temperature (red) peaks with PAR at 12:00.

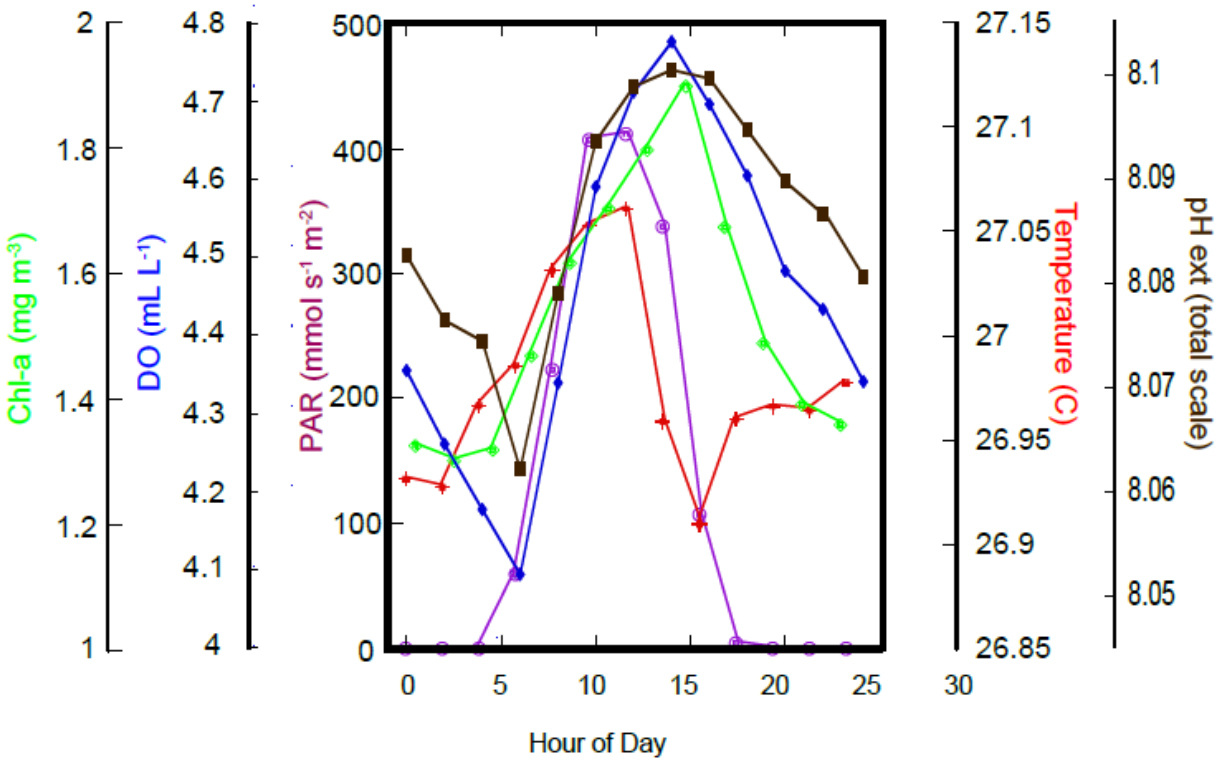

Fig. 15 The average values of select parameters over Week D (June 8 – June 14) are shown. Note the strong correlation between DO (blue) and pH (brown). Temperature (red) peaks along with PAR at noon.

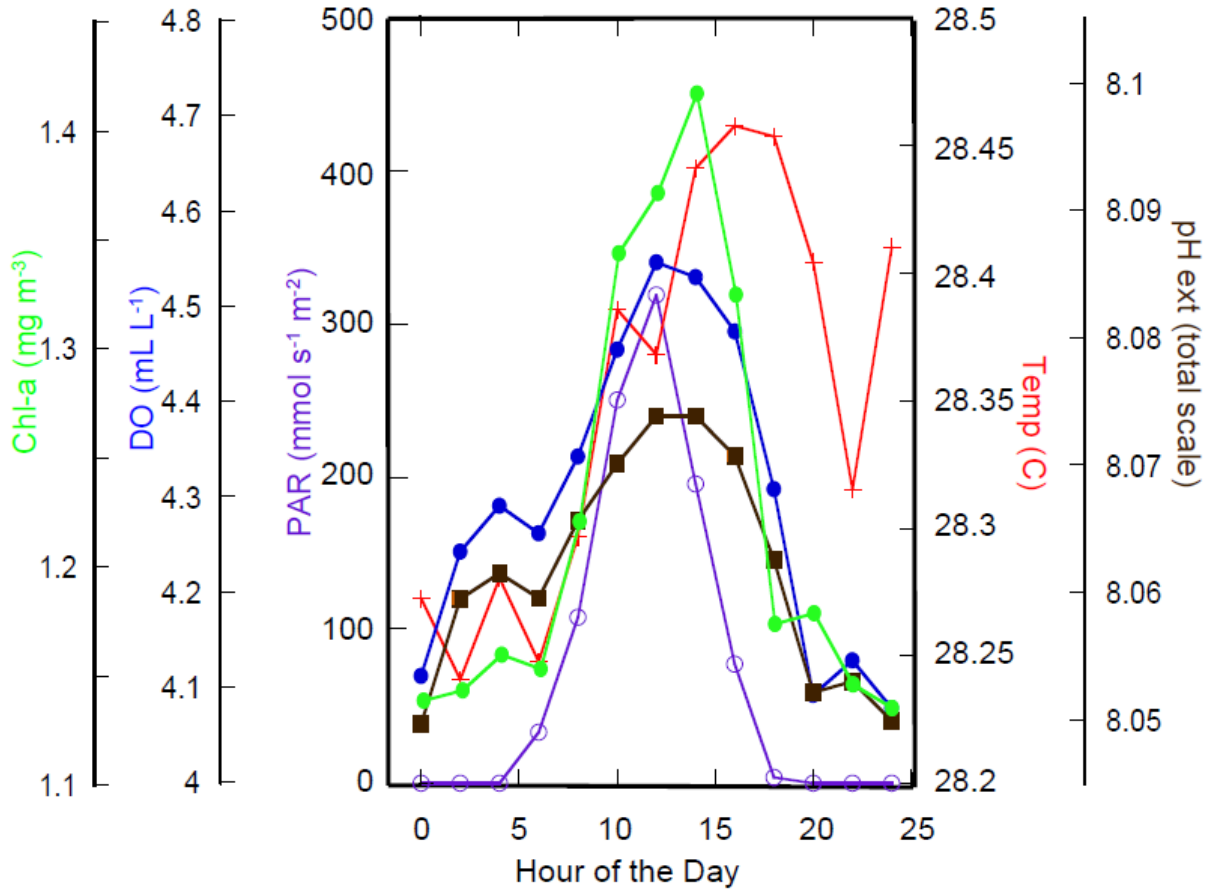

Fig. 16 The average values of select parameters over Week E (June 22 – June 28) are shown. Note the strong correlation between DO (blue) and pH (brown). Temperature (red) peaks last at 16:00.

during this season. Thus the ability to identify periods of major irregularity or unusual disturbance depends on having already discerned baseline patterns. To quantify the regularity of the various parameters' daily cycles, we propose that a higher order coefficient of variation is needed. Thus we define a new measure we call Hourly Variability (HV), for which the hourly standard deviations of a parameter in an "average day" are averaged together. The Relative Hourly Variability (RHV) divides this value by the average day's range and multiplies by 100%. Table 4 includes the results of these calculations.

What do RHV values indicate about the nature of a parameter's daily variability? Standard deviation values express variability *across* days, and dividing by the average day's range puts the value in context of typical variability *during* the day (and helpfully constrains the value as a percentage that is more comparable across time and parameters). For example, relatively high standard deviations and hence greater RHVs would exist if a pattern starts at a different time each day (e.g., see pressure RHVs below), or if there is an overarching trend in the values of a parameter (e.g., see temperature RHVs below). If a similar (in starting time, period, amplitude, etc) pattern exists, the RHV provides a cumulative measure of how much of the average daily range is due to such variations across the whole time span, with the rest of the variation attributable to changes within the daily cycle. This statistic encapsulates in one value the variability through time over an established period (in this case one week).

For an illustration of this concept from our data, consider Fig. 17. Each day's DO values are graphed as various colors, and averages taken at each time point compose an average day (black dotted line), whose range is 0.61 mL L^{-1}. DO seems to experience a very regular decline from 4.7 to 4.3 mL L^{-1} each day from 14:00 to 24:00, but many different values are visible during the period from 00:00 to 12:00. The standard deviations are shown with solid black error

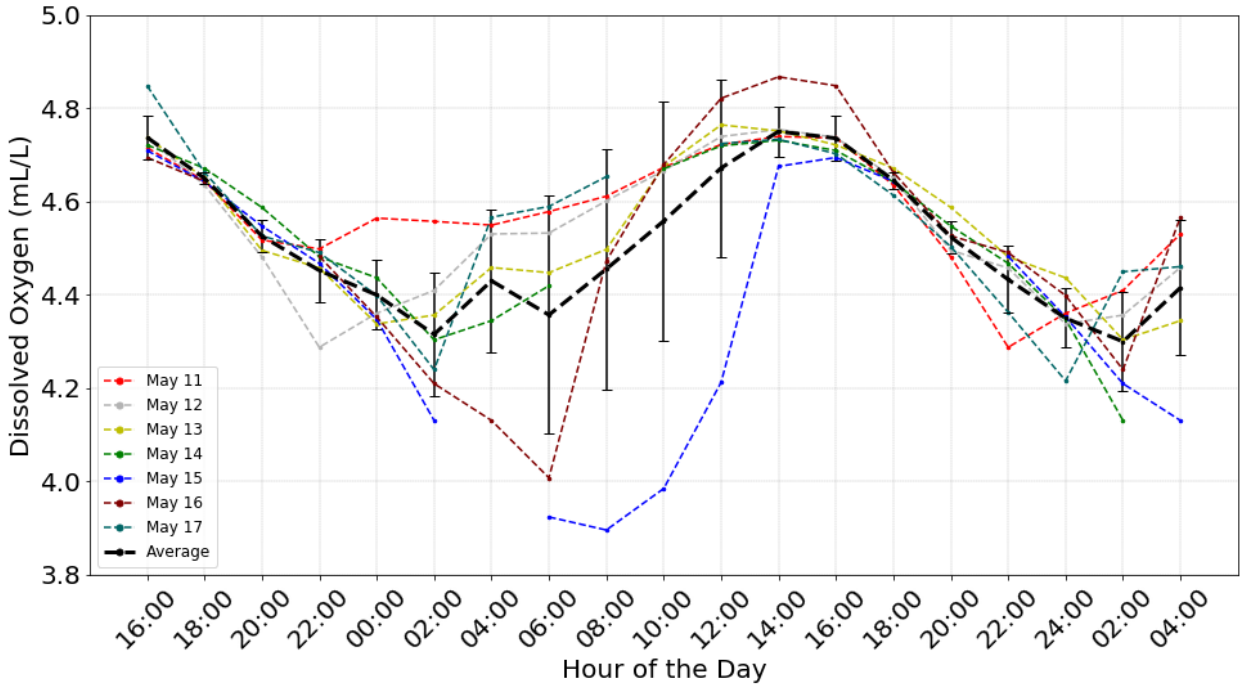

Fig. 17 Dissolved Oxygen data during the week of May 11 (Week A) are displayed. The average value at each time point is depicted by the dotted black line and its standard deviation with solid black error bars. The average of these standard deviations divided by the dotted line's range is defined as the Relative Hourly Variability.

bars, and are averaged together to find this week's HV: 0.11 mL L^{-1}. The RHV of DO data collected during this week is 0.11 / 0.61 * 100% = 17%. This regular pattern of roughly concurrent and congruent minima and maxima each day produces an RHV with a relatively small value.

We find RHVs to be most meaningful when their values are small because they quickly indicate that a pattern occurs each day with a similar range and timing. Our data produces examples at both high and low extremes: PAR always has a very low RHV (all < 10%) while the Chl-a has a high RHV (77%) during Week A. PAR is consistently near zero for ~10 hours each night and had a peak (with a roughly consistent absolute value) at either noon or 2PM; the Chl-a fluorescence values steadily increased from zero during Week A, eventually developing into a cyclic pattern between about 1 and 2 mg m^{-3}. This anomalous behavior is examined more closely later in this section, but that there are significantly different values each day is reflected by a high RHV and illustrative of the concept. Once it achieves cyclicity (Figs. 13 – 16), the Chl-a RHVs average a low 17%.

A close look at the statistical characteristics of the temperature data shows that this concept applies well to the behavior of temperature during our study period, which is under one aspect regular and another irregular. During the course of the study, not only did the temperature increase (+2.27 ± 0.75 C; Table 2), so did the average range and standard deviation of daily temperatures (Table 4). Thus, the range's RSD remained quite stable over the whole study period at 27 – 30%. Temperature's RHV decreased over the study period, indicating that the latter days were more similar to each other at each time point than the earlier days. The temperatures' RHVs are among the highest measured (35 – 79%): during this time period when the region's temperature is increasing regularly from greater insolation, each day and each week is

progressively warmer at EFGB (Fig. 18). Even when the RSD of the day's range is typical (~30%), the consistently high RHVs (≥35%) indicate that the temperature is changing day-by-day, as do graphical representations and linear regressions (Fig. 9; $R^2 = 0.92$ and 0.84 for SBE16 and SeapHOx thermometers respectively). Both facts (i.e. temperatures increasing week-by-week and the timing of the daily temperature cycle having no regular phase) lead to higher RHVs.

A statistical analysis of salinity displays the behavior of a conservative water property, as expected at this shelf-edge site with waters characteristic of the open Gulf. Its average daily range is typically less than 0.3 psu and is significantly greater only when different water masses are known to be influencing the study site (i.e. fresher water from Cindy; Week E in Table 4). Salinity exhibits RSDs almost identical to that of temperature (27 – 31%) but no diurnal cycle. Even during the week of June 22 (during which the site was recovering from a 2 psu drop due to Tropical Storm Cindy) while its daily average range is 3-7x greater than the prior weeks, its RSD is unchanged. The weeks with high RHVs exhibit at least one step change over the course of the week (see Fig. 5; May 11 = 0.3 psu, RHV = 43%; June 8 has three 0.1 psu steps, RHV = 45%; compare to other RHVs of 27, 28, and 33%), indicating that RHV does indeed measure similarity across days well. As mentioned above, Week E shows much salinity variability (an average daily range triple that of the other weeks at 0.78 psu), but achieves a lower RHV of 27%, as the strong variability is present each day, not in an isolated step-change.

The pH shows no such drastic changes, but does have a regular daily cycle, reflected in its RHVs typically around 20%. The pH-internal and -external sensors have an identical average RSD (27%), but a slightly different average RHV (22% vs 26%). pH-external's values should vary more than pH-internal's overall, because the data processing for the pH-external values

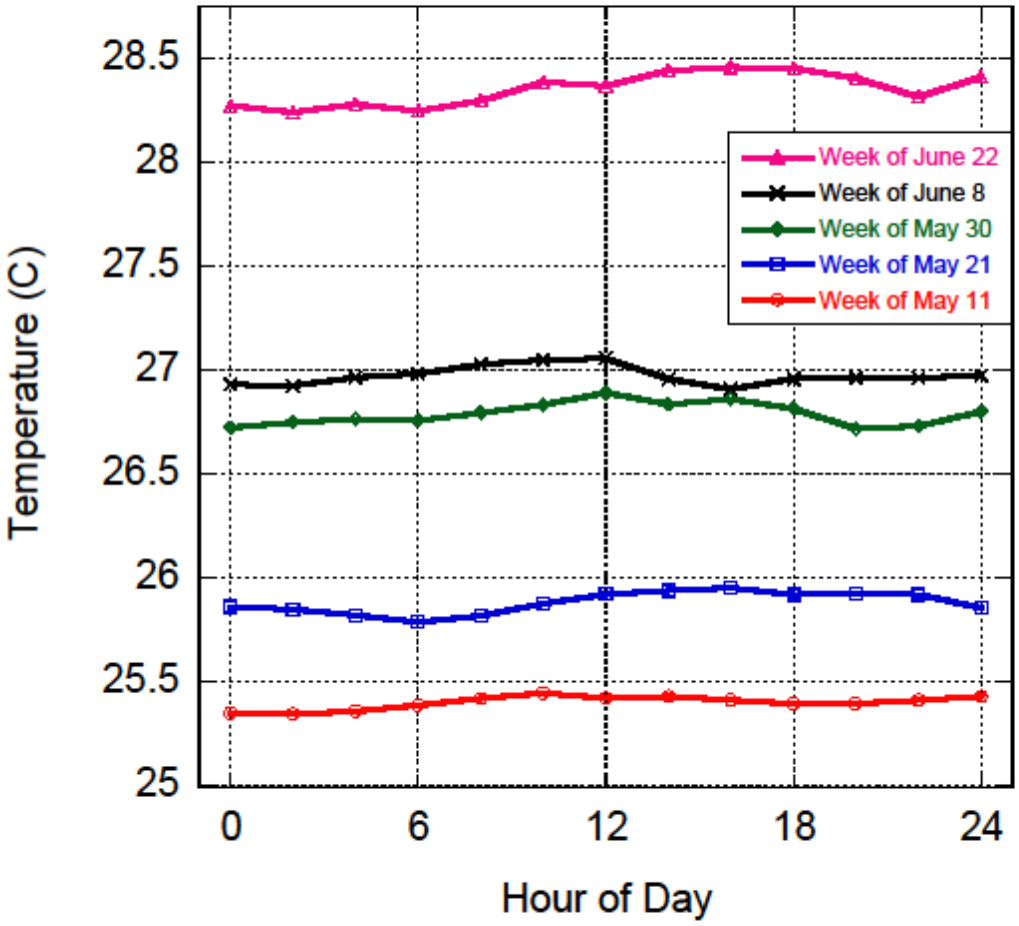

Fig. 18 Average daily temperature cycles for Weeks A-E are displayed. Week of May 11 is Week A (red); Week of May 21 is Week B (blue); Week of May 30 is Week C (green); Week of June 8 is Week D (black); Week of June 22 is Week E (pink).

involves corrections for salinity in addition to the temperature effects factored into the pH-internal processing. These slightly different processing regimens result in slightly different RHV values, fitting well with our understanding of how the sensors and their software operate.

The most regular cycle consistently present in our data is in the PAR values. The timing of the PAR pattern is regular: the peak occurs at 8 AM on 1.9% of the days, at 10 AM on 42.3% of the days, and 12 PM on 55.8% of the days and then falls to zero for ~10 hours each night. This long, recurring period of consistent behavior makes the RHVs consistently small: PAR exhibits the lowest RHVs of all measured variables. Even during weeks with the largest variability in the magnitude of peak radiation (Weeks B, C, and E have 4, 5, or 6 cloudy days (where PARmax <400 mmol $m^{-2}s^{-1}$)), the RHVs stay consistent and never rise above 10%. It should be noted that the structure of the "day" utilized makes these RHVs smaller than they otherwise would be: the extension of the day before 00:00 and after 24:00 double counts the late-night hours when PAR is always near zero. This does not invalidate these values, but shows how, in an extremely regular behavioral situation, RHVs behave as outlined above.

Turbidity was expected to be one of the most irregularly cycling parameters. Increases in its reported values would be caused primarily by increased resuspension of fine seafloor sediment, which is unpredictable and not expected to be regular. Almost no spikes at all were recorded; the value surpasses 0.5 NTU six times (only once for two consecutive data points) with a maximum of 2.42 NTU. With this very unremarkable dataset, its RHVs (average = 22%) are middling and not meaningful: not as low as those of the highly cyclic PAR or as high as those of the erratic temperature.

CDOM is the parameter with the most apparently random and irregular behavior. No daily variability is present in either graphical representations or RHV values (which are

consistently near 30%). The decrease in CDOM's mean from Week A to Week E (2.13 mg m^{-3}) is basically the same as the average standard deviation of the five weeks (2.08 mg m^{-3}). To better discern longer term trends in this data, a moving average with a Parzen window of 23 points is applied (Fig. 19). This window length filters out daily trends, and reveals some irregular periodicity. However, no correlation with a weekly timescale or pressure variability is present. There is too much noise in this data subset, and too much irregularity of behavior to deduce any additional meaningful conclusions or trends.

Pressure shows a regular cycle, with RHVs slightly higher than Chl-a and DO, which matches the different time scales: Chl-a and DO are driven by the 24-hour solar cycle, while pressure is driven by tidal cycles, which is based on a 24 hour - 50 minute lunar cycle. Each 'day' the RHV calculation is based on starts 24 hours after the previous 'day' starts, so this small offset between the period of pressure's cycle and the RHV 'day' inflates its RHVs.

To detail its aforementioned anomalously high RHV during Week A, the Chl-a fluorescence exhibits some mystifying behavior: an inexplicable ramping up of the signal during the first week. For most of the study period, the Chl-a values cycle daily between 1 and 2 mg m^{-3}, values typical of the site: on May 27, 2010 at 12:21 local time, the Chl-a was measured to be 2.1 mg m^{-3}, and below detection limit (1 mg m^{-3} Chl-a for discrete water samples) during each May since 2010 (personal communication with FGBNMS Staff). However, during the very beginning of data collection (the first ~14 days including Week A), the fluorescence values begin near zero and very slowly increase, gradually exhibiting a cyclic pattern. No satisfactory explanation for this fluorescence phenomenon has been forthcoming, either from discussions with the manufacturer, analysis of larger weather patterns, considerations about deployment conditions or comparison with temperature, dissolved oxygen, and other data. The other

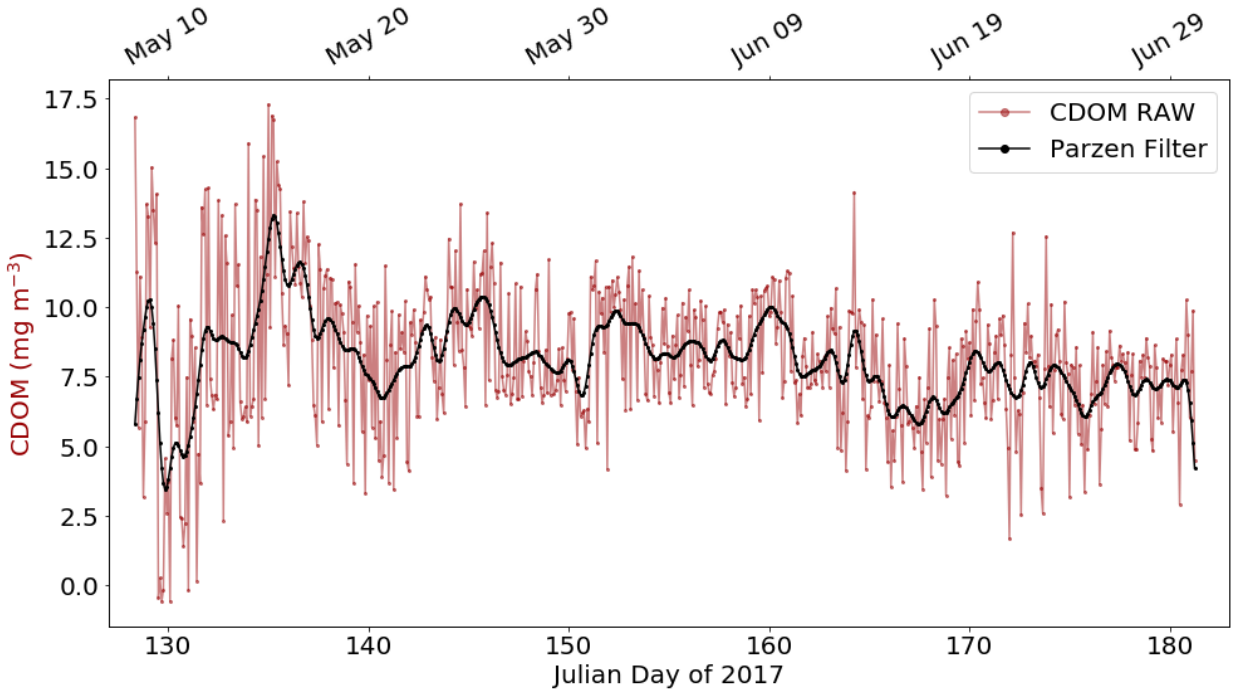

Fig. 19 CDOM data overlaid with a Parzen Filter. This filter uses a window length of 23 data points (two days) to filter out any daily trend.

parameter (turbidity) measured from the same sensor has a similarly anomalous period at the start of the deployment but seems to start functioning properly a week before the Chl-a signal cycles regularly. Keeping the detection limit in mind, it may be the case that the steadily increasing values of the first two weeks are accurate.

The Chl-a fluorescence shows an expected temporal correlation with PAR (notwithstanding its correlation coefficient of -0.1 from Table 3). Chl-a peaks typically follow closely on those of PAR (Figs. 12 – 16; Table 4), indicating that either chlorophyll fluoresces more strongly during peak sunlight hours, more chlorophyll is present during those hours or both. Some days have double peaks of fluorescence that indicate Chl-a quenching, but these do not correlate with days of peak irradiation (PAR > 400), as suggested by Marra (1997) (Fig. 20). More often, a double peak of Chl-a correlates with a double peak of PAR: a double peak of PAR always leads to a double peak of Chl-a, but sometimes Chl-a double-peaks without a PAR double peak or high PAR values. A larger dataset or even finer temporal resolution would be necessary if there are any further conclusions about this relationship to be drawn.

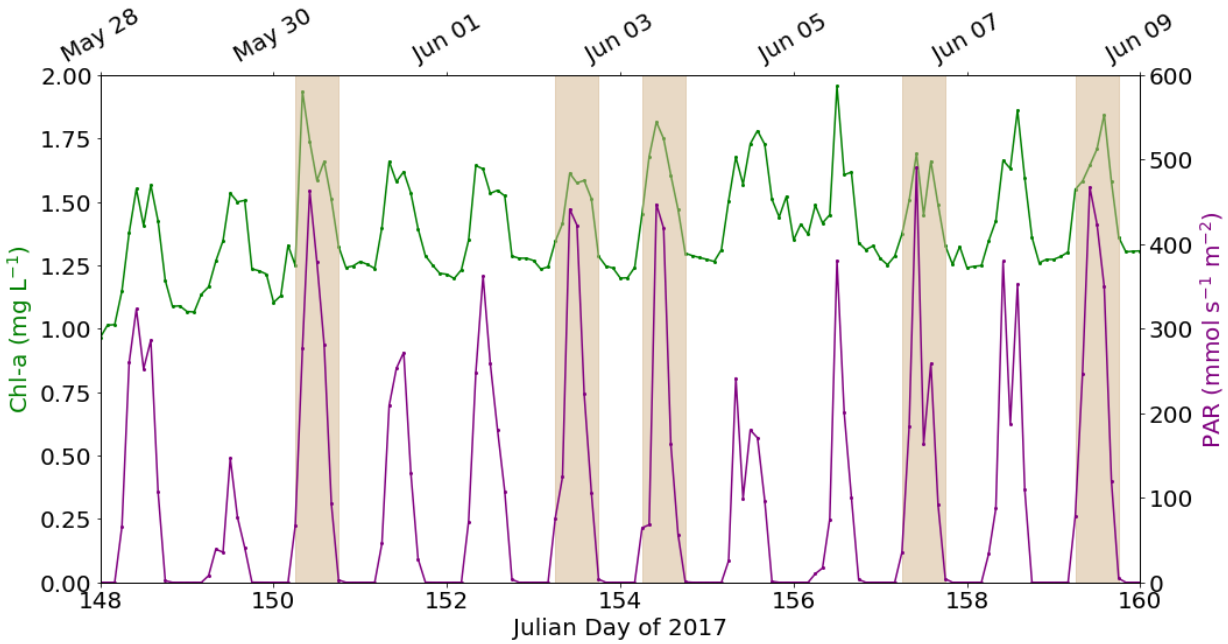

Fig. 20 PAR and Chl-a show a high degree of temporal correlation. Days of high irradiance (PARmax > 400 mmol $m^{-2}s^{-1}$) are shaded. Numbers on X-axis show midnight starting a given Julian Day. Double peaks of Chl-a are visible with (e.g. JD 150 and 157) and without (e.g. JD 148 and 151) high irradiance. Numerous high irradiance days occur without a double peak in Chl-a (e.g. JD 154 and 159). Some days exhibit a double peak of Chl-a and PAR (e.g. JD 148, 155 and 157) while some days exhibit a double peak only one parameter (e.g. JD 151).

6 DISCUSSION

During the time period of this study, the parameters measured at EFGB displayed two primary types of regular variability, the first during the overall spring to summer seasonal transition and the second during daily timescales. Some changes in parameters also occurred at irregular intervals, particularly with the passage of tropical storm Cindy towards the end of the study period.

Fig. 21 shows how SeapHOx temperature and pH varied over the entire study period. An overall increase in temperature occurred whereas an overall decrease in pH occurred. For the sake of statistical robustness and to enable comparison, these changes can be quantified two ways: by averaging the first and last 12 points (i.e. 24 hours) of data and by fitting a linear regression to the data. For temperature, these methods respectively yield increases of 2.27 and 3.32 C (R = 0.958). This increase is similar to changes observed previously during the spring to summer transition at the Flower Garden Banks (e.g., Gittings et al. 1992). For pH external, the two methods yield decreases of 0.039 and 0.047 units on the total scale, and for our discrete samples analyzed in a laboratory, pH decreases by 0.05 units. A slight overall decline of pH has also been observed at other Northern Hemisphere sites within 5° latitude of EFGB during the spring to summer transition (summarized in Fig. 2g in Bates et al. 2014): 0.06 at BATS (Bates et al. 2012), 0.013 at Station ALOHA (Dore et al. 2009), and ~0.005 at ESTOC (Gonzalez-Davida et al. 2003). Naturally, there are numerous forces in this dynamic system that affect pH.

The change in temperature is a primary determinant of the overall change in pH. Given the average measured salinity, pressure, and nutrient concentrations during the study period and assuming unchanging values of pCO_2 (400 uatm), TA (2350 umol $kgSW^{-1}$) and DIC (2050 umol $kgSW^{-1}$) which are the average values obtained (see Table 2), the observed temperature change

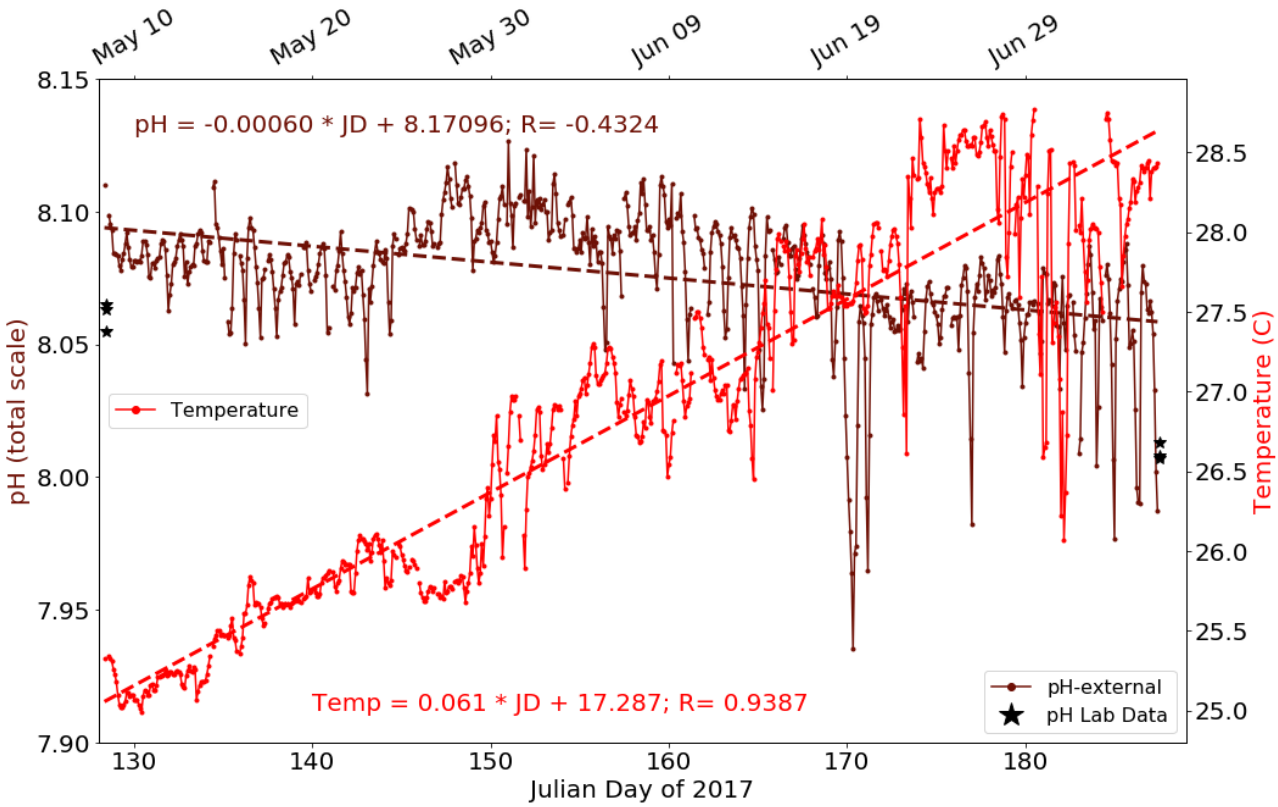

Fig. 21 Full temperature and pH during course of study are shown. SeapHOx thermometer and pH-external data shown.

from 25 C to 28.3 C would cause pH to decrease by 0.048 from 7.993 to 7.945. Temperature increases lead to pH decreases in the ocean, as carbonic acid, the primary buffering species, dissociates endothermically (i.e. a higher temperature pushes carbonic acid toward dissociation). Thus, the change in temperature alone can account for 100% of the net observed pH change.

Could another influence on the overall change of seawater pH be atmospheric CO_2? In the Northern Hemisphere, the concentration of atmospheric CO_2 varies on an annual basis (https://www.esrl.noaa.gov/gmd/ccgg/trends/). Fig. 22 shows that during 2016 and 2017, it reached its maximum at the observatory at Mauna Loa (MLO) during May. CO_2 is known to equilibrate slower than ordinary gases due to its chemical properties (Weiss 1970 and 1974), so the timescale for the upper ocean to come into equilibrium with the seasonal change in atmospheric CO_2 is months to a year. Due to the differences in concentrations, we would expect a net flux from the atmosphere into the surface of the ocean at the beginning of the study period (MLO = 409.65 ppm; EFGB calculated pCO_2 of 392.2 ppm) and from the ocean to the atmosphere by the end (MLO = 407.07 ppm; EFGB calculated pCO_2 of 450.1 ppm). Due to the depth of the study site and the relatively slow equilibration rate of pCO_2, it is far more likely that photosynthesis and respiration play a more significant role in the carbonate chemistry of EFGB.

At the seasonal scale, DO does not appear to drive the decrease of pH. DO exhibits no overall trend (slope of regression for the DO dataset is -0.0074 mL L^{-1} d^{-1}; R = -0.368) and is consistent with its saturation state, which also shows a negligible overall decrease with a slope of -0.0020 mL L^{-1} d^{-1} (R = -0.444). Long-term, the DO concentration is constrained: the site's close proximity to the sea surface normally prevents drastic deviations (Broecker and Peng, 1982), and we witness no long-term processes affecting it. The DO concentration (mean = 4.42 mL L^{-1}) is consistently just less than its calculated saturation state (mean = 4.80 mL L^{-1}; Fig. 23), indicating

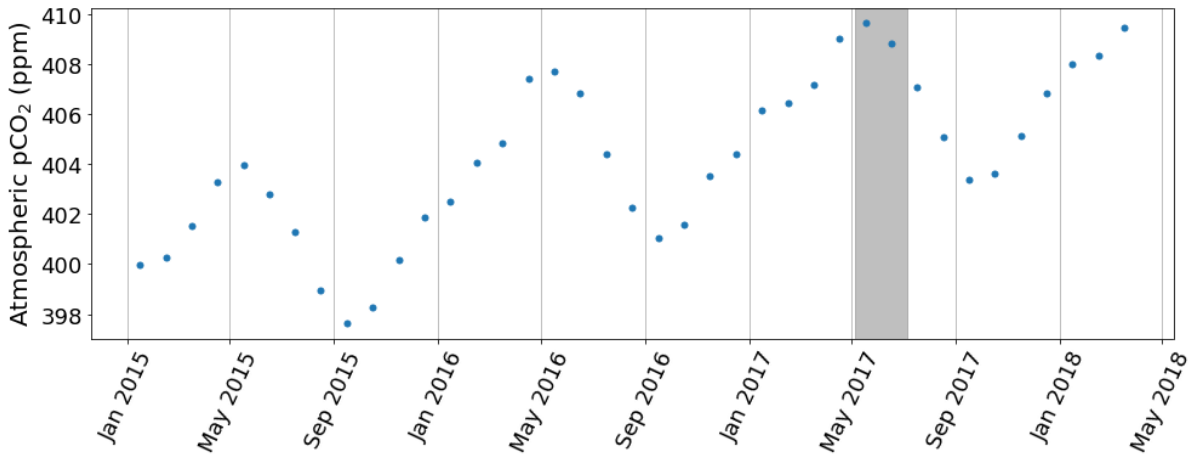

Fig. 22 The concentration of atmospheric CO_2 measured at Mauna Loa, Hawaii. This value varies annually and reaches peak levels during May. Our study period is highlighted in gray. Data taken from https://www.esrl.noaa.gov/gmd/ccgg/trends/graph.html.

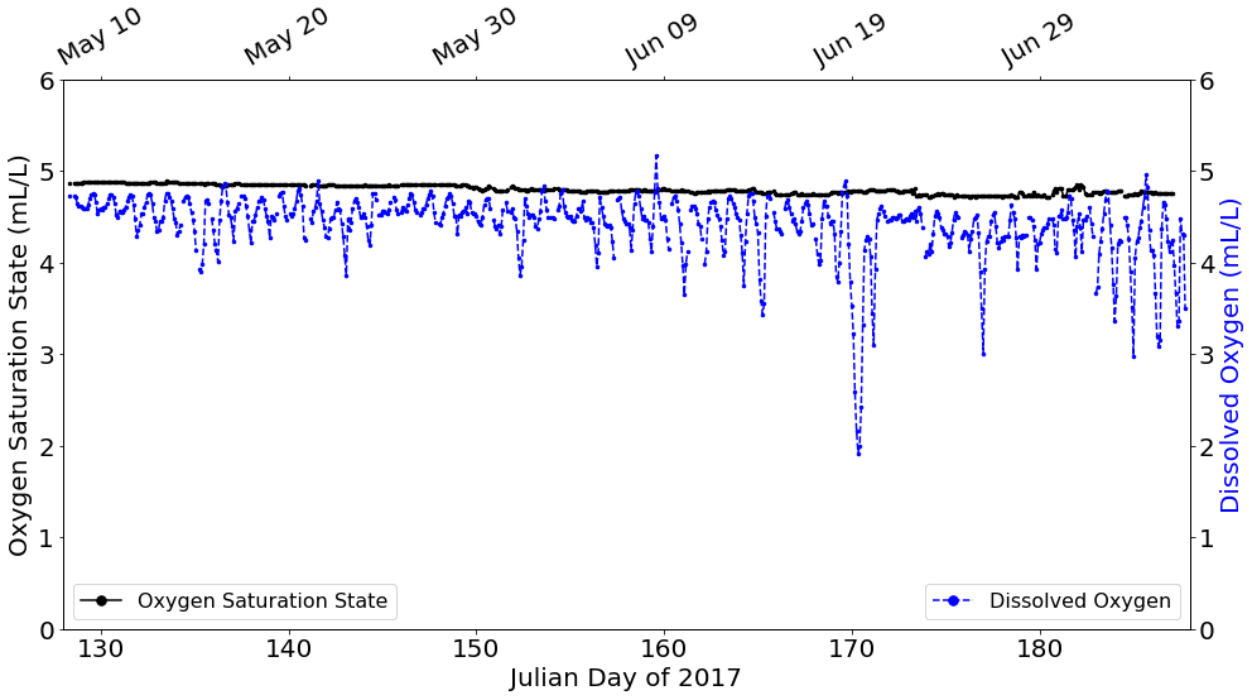

Fig. 23 Oxygen saturation state and concentration over the course of the deployment. Saturation state calculated using measured parameters, constants from Benson and Krause (1984), and equation from Garcia and Gordon (1992).

a possible calibration error, as we expect DO to be supersaturated in surface water. Whatever the true value of DO, the two parameters remain closely linked throughout the study period.

Several lines of evidence show a tight link between changes of DO and pH during short periods. There is a strong overall linear relationship between these parameters (R value of 0.917 at a lag of 0 hr, see Fig. 10; Table 3). Figs. 12-16 and Fig. 24 also display a close correspondence between daily variations of these parameters, which is confirmed by the consistent and low RHV statistics for DO (14-21%) and pH-int (19-27%). A similarly close relationship between DO and pH was observed in a coastal kelp forest where significant photosynthesis occurs by Frieder et al. (2012). We therefore attribute the tight bond between pH and DO to biological activity, as DO and inorganic carbon are a conjugate pair in the photosynthetic-respiratory equilibrium; Mostofa et al. (2016) found a strong inverse correlation between DIC and DO in a closed seawater system (Fig. 5c therein). This close pH-DO relationship has been shown to be pronounced in estuarine, shallow, and otherwise constrained environments, and in ecosystems of high biological productivity (e.g. Yates et al. 2007; Dai et al. 2009; Drupp et al. 2013). Biological activity plays a dominant role over the short-term at EFGB, a relatively open-ocean site at a depth of 22 m on the continental shelf-slope break, especially in the cycles of pH and DO and in the absence of other factors such as groundwater flux, terrestrial influences, large tidal ranges, and chemical limitations such as hypoxia or extreme alkalinity.

There is a regular structure to the standard daily cycles of several important parameters at EFGB. We use calculated lag times to anchor the relative timing of various daily cycles to that of PAR. PAR peaks at either 10 AM or noon (98% of the time) and Chl-a peaks contemporaneously or two hours after. After PAR, both pH parameters peak with a lag time of two to four hours – both lag intervals have R values of 0.315 - 0.330 (relatively high R values for PAR). The DO

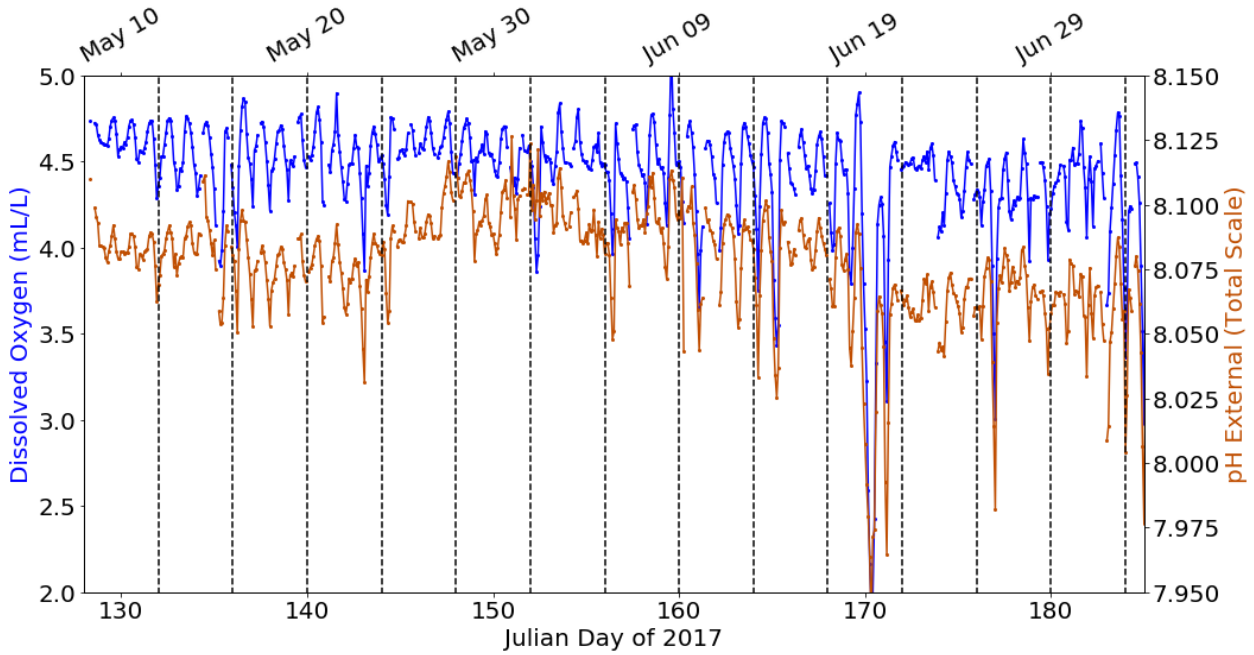

Fig. 24 pH and DO show coordinated daily cycles across the whole study period. A consistent direct correlation appears to exist between daily cycles of pH (brown) and DO (blue). Black lines added to guide the eye.

peak occurs four hours after that of the PAR (R = 0.392). As previously discussed, the DO and pH are closely linked during daily cycles. This matches with the 0 hour lag and 0.864 average R between pH and DO (Figs. 19 & 21). There is a direct correspondence between the daily insolation cycle and Chl-a fluorescence values evident in Figs. 12 – 16. Consistent with this observation, both Chl-a and PAR have very low RHV values (Table 4), indicating regular cycles of both parameters.

Temperature exhibits a daily cycle, but some inconsistency exists in its relationship to daily cycles of other parameters. Temperature begins to rise at about the same time as PAR; however, the peak of temperature lags behind pH-ext and DO by 6 – 8 hours and temperature's R values with pH-ext and DO are only 0.387 and 0.33, respectively. That the peak temperature lags the peaks of other parameters is consistent with seawater's high specific heat capacity – it does not heat or cool quickly. Temperature's RHV is elevated relative to other parameters that exhibit a daily cycle because its peak doesn't always occur at a specific time – weekly average temperature values (Table 4) peak prior to (Fig. 12), contemporaneously with (Figs. 14 & 15), or after PAR (Figs. 13 & 16). The inconsistent timing of the daily temperature cycle and temperature's poor correlation with PAR may reflect several factors. The daily range of temperature is typically only about 0.15 to 0.2 C and, in addition to PAR, it is influenced by processes such as vertical mixing and air-sea exchange. As a result, temperature does not cycle as neatly as parameters such as PAR, pH, and DO that are closely linked to either solar forcing, biological mediation, or a combination thereof.

Parameters that are either driven by or closely linked to biological activity have characteristically regular daily patterns, as reflected in small RHVs. The RHV statistic is a good measure of the regularity of patterned behavior over a given time with meaningful gradations of

its values. PAR, the most consistently cycling parameter has remarkably low RHVs that are always single digits. Chl-a, DO and pH (parameters affected by multiple external influences) have slightly greater RHVs (14 – 35%). Pressure's RHVs are slightly higher than PAR's (13 – 23%), reflecting the fact that its cycle is out of phase with the imposed 24 hour window. Although temperature exhibited a daily cycle, its timing was less regular, and thus has RHVs similar to CDOM and salinity (26 – 43%). These latter physical parameters do not cycle as neatly as the biologically-linked parameters and have correspondingly high RHVs. Salinity's typical daily ranges are dwarfed by weekly variability (Fig. 25). Thus, when establishing baseline data for typical conditions at a study site, the RHV statistic can show how regular patterns are and is comparable across parameters. Although other sites may have different baseline values, suggested classifications based on this study are RHV $\leq$ 10%: highly regular; 10% < RHV $\leq$ 25%: regular; 25% < RHV $\leq$ 35%: somewhat irregular; RHV $\geq$ 35%: irregular.

The RSD statistic is more useful for individual parameters than for making comparisons between different parameters' patterns. As the average temperature increases (Fig. 18), the daily SD increases proportionally; thus temperature's RSD remains constant: compare Week B (avg temp range = 0.273 C; std dev = 0.078 C; RSD = 29%) to Week D (avg temp range = 0.629 C; std dev = 0.180 C; RSD = 29%). Although EFGB corals typically experience temperatures approaching 30 C every summer (Schmahl et al. 2008), if the temperature behavior that we observe is typical, then organisms at the site can be expected to experience a greater range of temperatures on a daily basis as hotter seasons get even hotter.

External forcing may play a role over the medium-term in causing irregular parameter behavior. Step changes of salinity may indicate passage of marine fronts that bring in new water masses that differ in either pH or DO (e.g. cyan, yellow, and pink zones of Fig. 5). The

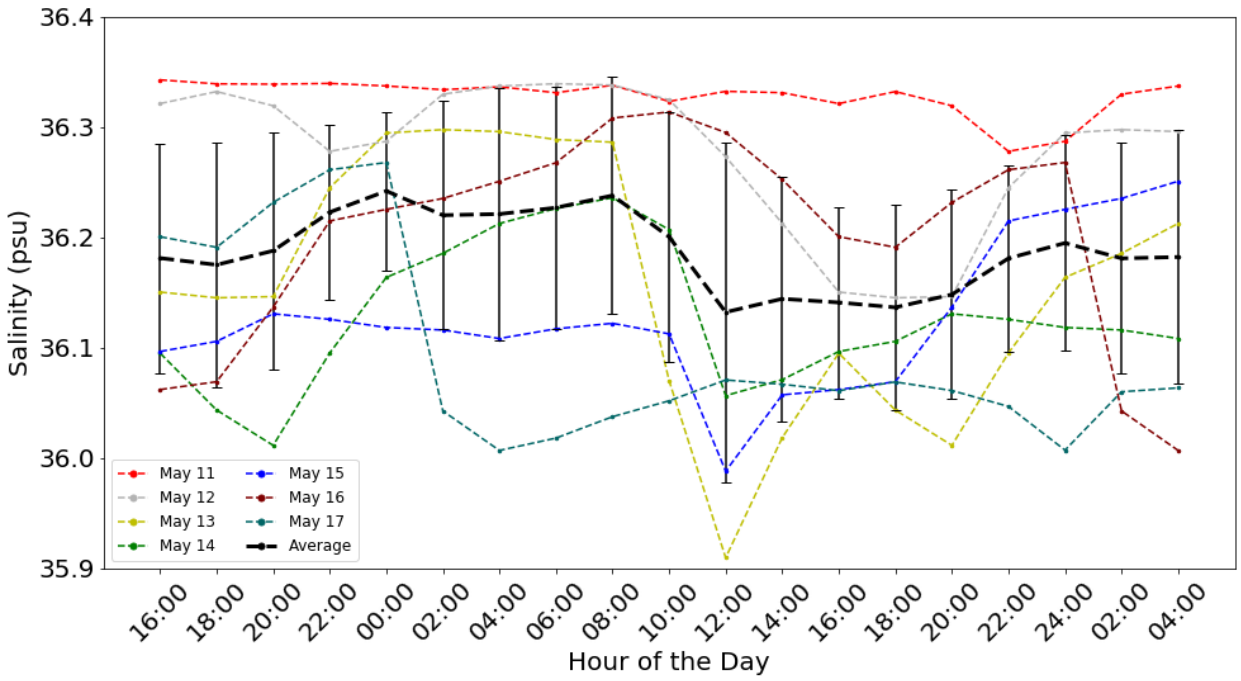

Fig. 25 Salinity data during the week of May 11 (Week A). Standard deviations are shown with solid black error bars: no daily trend is visible during this week or any other so analyzed.

introduction of near-surface water – typically supersaturated with DO (Broecker and Peng) – or waters from below the mixed layer – expected to be lower in DO due to respiration over time – could be indicated by these salinity changes (which correlate with increased wind gustiness, see Fig. 6). Salinity instabilities match with other evidence for intense vertical mixing during Tropical Storm Cindy, including increased variability between temperature and salinity sensors, and a dramatic storm-driven freshening (Figs. 4 and 5 pink zone). During periods of normal weather, effects of variable wind-driven vertical mixing at the EFGB reef crest are less apparent. On the daily/weekly scale, salinity and wind gust data (the latter smoothed with a two hour weighted average) visually appear to show a slight direct temporal correspondence (higher winds and salinity during first part of day); yet, calculated correlation coefficients are small (Fig. 26). The magnitude of variability of these parameters is small, and their relationship is not simple. Given the present lack of data about current velocity, potential topographic effects, and uncertainty regarding the local vertical profiles of salinity in the water column (e.g. Teague et al., 2013), a more in-depth study is needed to assess the relation between wind speed and salinity.

Other than vertical mixing, the only other potential source of nutrients at this location, apart from *in situ* remineralization, is land runoff, which we do not expect at this depth so soon after the storm. This Cindy-influenced surface water, expected to be cooler, less saline, and higher in nutrients, seems to be in the process of mixing at the coral cap, though not quickly reaching equilibrium. This event should not pose a danger to the biota of the reef, as the RSDs of temperature and salinity (i.e. short-term variability experienced by the reef crest) during the aftermath reflect normal conditions of near 30% (Table 4). Despite the effects of Cindy, the overall carbonate chemistry trends observed at EFGB match our understanding of the site's seasonal behavior and behavior observed at similar sites.

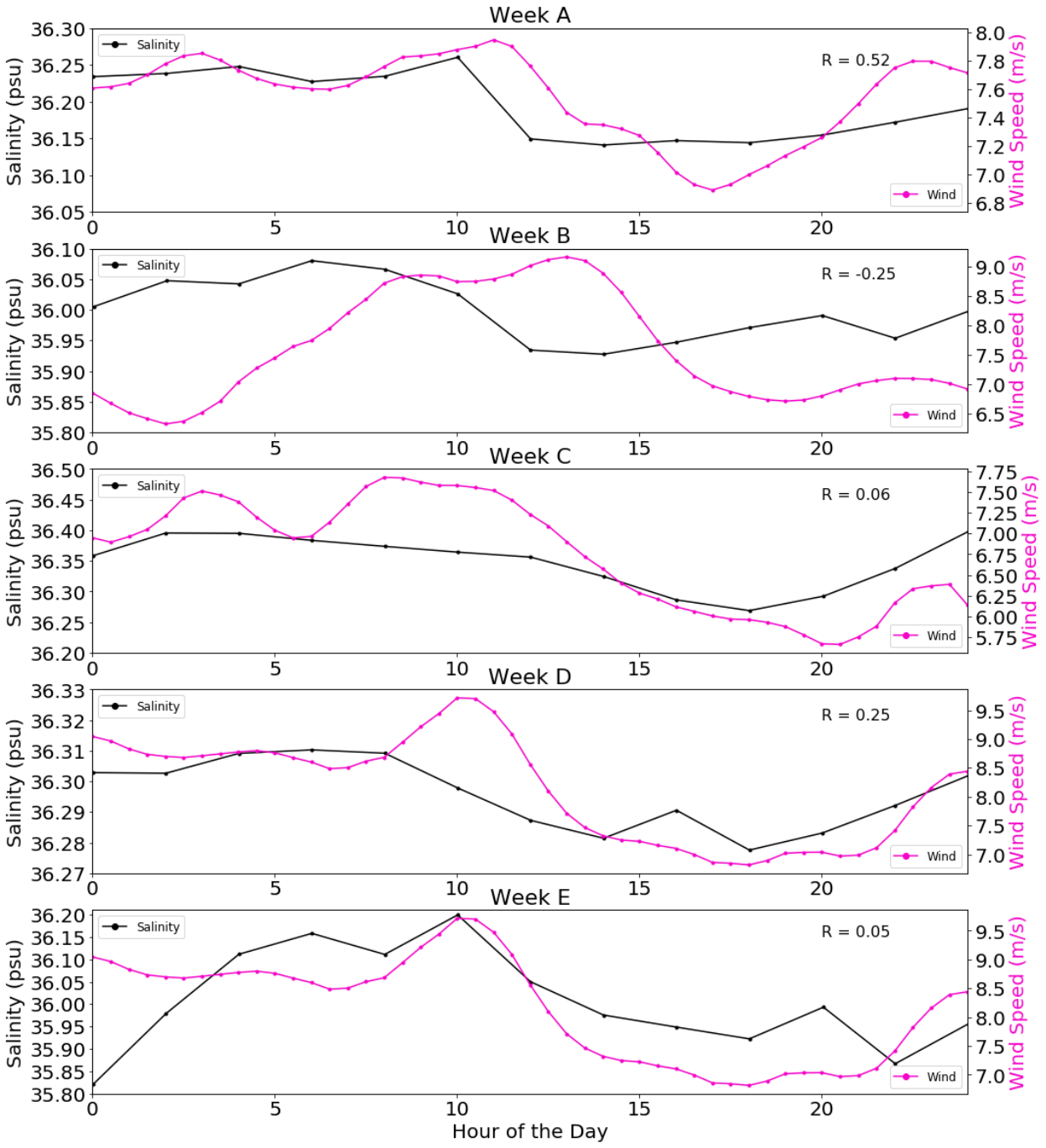

Fig. 26 Average days of salinity and wind gust data during Weeks A – E correlate weakly. Wind data are the seven day average of the wind gust speed smoothed with a two hour triangular-weighted filter. The R value listed in each interior graph is that of a linear relationship between contemporaneous salinity and wind data for the average day (N = 12). While daily minima and maxima are visible for each parameter during each week, the ranges are much smaller than standard deviations.

No large change of nDIC, Ω_{arag}, or nTA values was measured. Discrete seawater samples collected at the beginning and end of the study indicated nTA increased by 55.9 umol kg^{-1} (~2%) and nDIC increased by 60. umol kg^{-1} (~3%). Calculated from the discrete samples' other carbonate parameters, the pCO_2 increased by 57.9 ppm and Ω_{arag} decreased by 0.04 (~1%). These data are in agreement with each other and standard changes in similar regions' seawater chemistry: monthly time-series from HOT, BATS and ESTOC averaged over at least 20 years (summarized in Bates et al. 2014) show seawater's pCO_2 increasing to reach an annual maximum during the late summer (Fig. 2e), nDIC slightly decreasing (Fig. 2d), and Ω_{arag} holding steady or ever-so-slightly increasing (Fig. 2h) over this period at subtropical sites in the Northern Hemisphere. BATS, specifically, reported an increase in the surface ocean concentration of 63 ppm pCO_2 (preliminary data) from 419 to 482 ppm from May 6 to July 6, 2017 (Fig. 27).

We show that the biological community at EFGB has a measurable effect on its marine environment. The frequency of daily pH cycles at our study location is similar to, but the absolute value of the cycle (0.03 – 0.05) is substantially less than, observations at shallower, coastal reefs (e.g. 0.22 – 0.29 at Tampa Bay and Florida Bay – Yates et al. 2007), at sites affected by upwelling (e.g. 0.2 – 0.4 at Monterey Bay – Booth et al. 2012), and at reefs and their terraces in the equatorial Pacific (e.g. 0.12 – 0.25 at Palmyra Atoll – Hofmann et al. 2011). The significance of the benthic signals we report is quite notable, given that the large volume of seawater in the immediate vicinity of the surface area of EFGB and rapid rate that it exchanges with the open ocean will tend to dampen the daily range of pH. Moreover, the shelf-edge location of the EFGB isolates it from influences of natural and anthropogenic coastal processes. If organisms at the Flower Garden Banks are adapted to low pH variability during a typical day, they may be more vulnerable to large pH changes in the future; however, this site's great

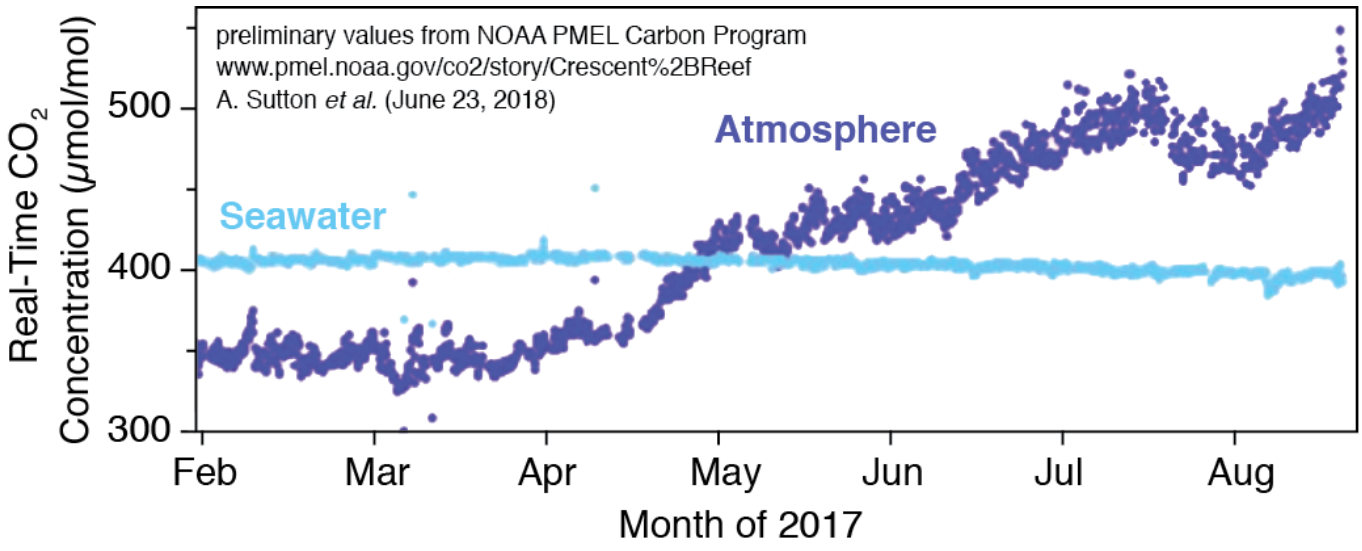

Fig. 27 Seawater and atmospheric pCO_2 at Crescent Reef near BATS. An increase in the former during the months of May, June and July is evident.

seasonal and interannual/interdecadal variability (e.g. Bright et al. 1984; Slowey and Crowley 1995; Wanninkof et al. 2015) may produce hardier species that adapt well to a changing ocean. Over the long-term, additional data from this site is required to produce a clearer picture of open-ocean ocean acidification and shed light on its effects on EFGB's healthy reef community. Thus, further study of the physical and geochemical processes at the Flower Garden Banks is necessary.

7 CONCLUSION

During the transition from May to July 2017, carbonate chemistry changes at EFGB were more subdued than those that have been observed at shallower, coastal coral reef environments; nevertheless the biology of the reef and ambient seawater has clear daily impacts on the surrounding marine environment. pH variations are driven by photosynthesis and respiration on a short-term basis, shown in this study as a constantly tight correlation between pH and the concentration of DO. Over the seasonal period studied, the DO concentration is consistently near saturation, and the overall decline in pH (0.047 on the total scale) matches with the observed temperature increase of ~3.32 C. While this pH value is similar to the typical daily ranges of 0.03 – 0.05 units, the CO2SYS program (holding other parameters equal) produces a 0.048 unit pH decrease for this temperature increase. However, during any given day or week, the behavior of temperature is uncoupled from that of any other parameter, and the timing of peak temperature is unpredictable. In contrast, parameters directly related to or resulting from biological productivity exhibit a regular structure: PAR peaks either with or shortly before Chl-a fluorescence, and DO and pH reliably peak 2-4 hours after PAR.

The regularity of variations in each parameter's behavior is indicated clearly by the parameter's RHV. We are interested to see if future work undertaken at other locations finds RHV thresholds for environmental parameters that are similar to those that exist at EFGB.

Vertical mixing of surface water down toward the reef cap is evidenced during periods of quick, sharp salinity change paired with high wind activity, leading to increased variability between co-located thermometers and salinometers, and an uptick in nutrient concentrations. No period of extreme variability was found: RSD's of temperature, salinity, DO, pH, Chl-a fluorescence, and PAR always stayed near 30%.

As Drupp et al. (2013) stressed the differences of carbonate chemistry conditions among various reefs, the addition of this study at a relatively deep and non-coastal reef to the literature will be a boon to understanding the entire picture of historic and future oceanic carbonate chemistry variability. This having been said, the seasonal trends of pH (slight decrease), temperature (increase), Ω_{arag} (unchanged to slight decrease), and pCO_2 (increase) at EFGB during May – July correlate with studies done at coral reefs at similar northern latitudes.

REFERENCES

Andersson AJ (2014) The Oceanic $CaCO_3$ cycle, in: Holland HD and Turekian KK (eds.), Treatise on Geochemistry, 2nd edn. Elsevier, Oxford, pp 519–542

Bates NR, Best MHP, Neely K, Garley R, Dickson AG, Johnson RJ (2012) Detecting anthropogenic carbon dioxide uptake and ocean acidification in the North Atlantic Ocean. *Biogeosciences* 9:2,509-2,522 http://dx.doi.org/10.5194/bg-9-2509-2012

Bates NR, Astor YM, Church MJ, Currie K, Dore JE, González-Dávila M, Lorenzoni L, Muller-Karger F, Olafsson J, Santana-Casiano JM (2014) A time-series view of changing ocean chemistry due to ocean uptake of anthropogenic CO_2 and ocean acidification. Oceanogr. 27:126–141. https://dx.doi.org/10.5670/oceanog.2014.16

Benson BB, Krause D (1984) The concentration and isotopic fractionation of oxygen dissolved in freshwater and seawater in equilibrium with the atmosphere, Limnol. Oceanogr. 29:620-632

Booth JAT, McPhee-Shaw EE, Chua P, Kingsley E, Denny M, Phillips R, Bograd SJ., Zeidberg LD, Gilly WF (2012) Natural intrusions of hypoxic, low pH water into nearshore marine environments on the California coast. Cont. Shelf Res., 45:108–115

Bright T, Kraemer G, Minnery G, Viada S (1984) Hermatypes of the Flower Garden Banks, northwestern Gulf of Mexico: a comparison to other western Atlantic reefs. Bull. Marine Sci. 34:461-476

Broecker WS, Peng T-H (1982) Tracers in the Sea. Lamont-Doherty Geological Observatory of Columbia University, Palisades

Canadell JG, Le Quere, C., Raupach, M.R., Field, C.B., Buitenhuis, E.T., Ciais, P., Conway, T.G., Gillett, N.P, Houghton, R.A., Marland G (2007) Contributions to accelerating atmospheric CO_2 growth from economic activity, carbon intensity, and efficiency of natural sinks. Proc. Natl. Acad. Sci. 104:18866–18870

Cao L, Caldeira K, Jain AK, (2007) Effects of carbon dioxide and climate change on ocean acidification and carbonate mineral saturation. Geophys. Res. Let. 34:L05607

Cesar H, Burke L, Pet-Soede L (2003) The economics of worldwide coral reef degradation. Cesar Environmental Economics Consulting and WWF-Netherlands, Arnhem and Zeist, The Netherlands

Chan NCS, Connolly SR, (2013) Sensitivity of coral calcification to ocean acidification: a meta-analysis. Glob. Change Biol. 19:282–290

Cinner JE, JN Kittinger (2015) Linkages between social systems and coral reefs in Ecology of Fishes on Coral Reefs. ed. Mora, C. 215–220

Comeau, S, Carpenter RC, Edmunds PJ (2013) Coral reef calcifiers buffer their response to ocean acidification using both bicarbonate and carbonate. Proc. R. Soc. B. 280:20122374

Dai M, Lu Z, Zhai W, Chen B, Cao Z, Zhou K, Cai W-J, Chen C-T (2009) Diurnal variations of surface seawater pCO_2 in contrasting coastal environments. Limnol. Oceanogr. 54:3:735–745

Dickson A, Sabine C, and Christian J [eds.] (2007) Guide to best practices for ocean CO_2 measurements. PICES Special Publication 3

Dore, JE, Lukas R, Sadler DW, Church MJ, Karl DM (2009) Physical and biogeochemical modulation of ocean acidification in the central North Pacific. Proc. of the Nat. Academy of Sci. of the USA. 106:12,235–12,240 http://dx.doi.org/10.1073/pnas.0906044106

Drupp PS, De Carlo EH, Mackenzie FT, Sabine CL, Feely RA, and Shamberger KE (2013) Comparison of CO_2 Dynamics and Air–Sea Gas Exchange in Differing Tropical Reef Environments. Aquat. Geochem. 19:371-397 https://doi.org/10.1007/s10498-013-9214-7

Feely RA, Sabine CL, Lee K, Berelson W, Kleypas J, Fabry VJ, and Millero FJ (2004) Impact of anthropogenic CO_2 on the $CaCO_3$ system in the oceans. Science. 305:5682:362–366

Feely RA, Alin SR, Newton J, Sabine CL, Warner M, Devol A, Krembs C, and Maloy C (2010) The combined effects of ocean acidification, mixing, and respiration on pH and carbonate saturation in an urbanized estuary. Estuar. Coast. Shelf Science. 88:442–449

Frieder CA, Nam SH, Martz TR, and Levin LA (2012) High temporal and spatial variability of dissolved oxygen and pH in a nearshore California kelp forest. Biogeosciences. 9:3917–3930. https://doi.org/10.5194/bg-9-3917-2012

Garcia HE and Gordon LI (1992) Oxygen solubility in seawater: Better fitting equations. Limnol. Oceanogr. 37:6:1307-1312

Gattuso J-P, Frankignoulle M, Bourge I, Romaine S, and Buddemeier RW (1998) Effect of calcium carbonate saturation of seawater on coral calcification. Global and Planetary Change. 18:1–2:37-46. https://doi.org/10.1016/S0921-8181(98)00035-6

Gittings SR (1998) Reef community stability on the Flower Garden Banks, northwest Gulf of Mexico. Gulf of Mexico Science. 16:161–169

Gittings SR, Boland GS, Deslarzes KJ, Hagman DK, and Holland BS (1992) Long-term monitoring at the East and West Flower Garden Banks. US Dept. of the Interior, Minerals Management Service, Gulf of Mexico OCS Region, New Orleans, LA. OCS Study MMS, 92-0006

González-Dávila M, Santana-Casiano JM, Rueda MJ, Llinas O, and Gonzalez-D´avila EF (2003) Seasonal and interannual variability of seasurface carbon dioxide species at the European Station for Time Series in the Ocean at the Canary Islands (ESTOC) between 1996 and 2000. Global Biogeochem. Cycles. 17(3), 1076 doi:10.1029/2002GB001993

Gray SEC, DeGrandpre MD, Langdon C, and Corredor JE (2012) Short-term and seasonal pH, pCO_2 and saturation state variability in a coral-reef ecosystem. Global Biogeochemical Cycles. 26:GB3012. https://doi.org/10.1029/2011GB004114

Green RE, Bower AS, and Lugo-Fernández A (2014) First Autonomous Bio-Optical Profiling Float in the Gulf of Mexico Reveals Dynamic Biogeochemistry in Deep Waters. PLOS ONE. 9:7:e101658. https://doi.org/10.1371/journal.pone.0101658

Hagens M, Middelburg JJ (2016) Generalised expressions for the response of pH to changes in ocean chemistry. Geochimica et Cosmochim. Acta. 187:334-349

Hofmann GE, Smith JE, Johnson KS, Send U, Levin LA, Micheli F, et al. (2011) High-Frequency Dynamics of Ocean pH: A Multi-Ecosystem Comparison. PLoS ONE. 6:12:e28983. doi.org/10.1371/journal.pone.0028983

Jochens AE, DiMarco SF (2008) Physical oceanographic conditions in the deepwater Gulf of Mexico in summer 2000-2002. Deep Sea Res. (Part II, Topical Studies in Oceanography). 55:24-26:2541-2554

Keeling CD, (1973) The production of carbon dioxide from fossil fuels and limestone. Tellus. 25:174-198

Keeling CD, Piper SC, Bacastow RB, Wahlen M, Whorf TP, Heimann M, and Meijer HA (2001) Exchanges of atmospheric CO_2 and $^{13}CO_2$ with the terrestrial biosphere and oceans from 1978 to 2000. I. Global aspects, SIO Reference Series. No. 01-06. Scripps Institution of Oceanography, San Diego, 88 pages.

Liddell WD, Ohlhorst SL (1988) Proceedings of the 6th International Coral Reef Symposium. 3:281-286

Marra J (1997) Analysis of diel variability in chlorophyll fluorescence. Journal of Marine Res. 55:767-784

Martz TR, Connery JG, and Johnson KS (2010) Testing the Honeywell Durafet for seawater pH applications. Limnol. Oceanogr. Methods. 8:172-184

Millero FJ, Pierrot D, Lee K, Wanninkhof R, Feely R, Sabine CL, Key RM, and Takahashi T (2002) Dissociation constants for carbonic acid determined from field measurements. Deep-Sea Research I. 49:1705–1723

Moberg F, C. Folke (1999) Ecological goods and services of coral reef ecosystems. Ecological Economics. 29:2:215-233

Morse JW, MacKenzie FT (1990) Geochemistry of Sedimentary Carbonates. Developments in Sedimentology. 48:1–707

Mostofa KMG, Liu C-Q, Zhai W, Minella M, Vione D, Gao K, Minakata D, Arakaki T, Yoshioka T, Hayakawa K, Konohira E, Tanoue E, Akhand A, Chanda A, Wang B, and Sakugawa H (2016) Reviews and Syntheses: Ocean acidification and its potential impacts on marine ecosystems. Biogeosciences. 13:1767–1786

NOAA Coral Program (2014) NOAA Coral Reef Conservation Program National Coral Reef Monitoring Plan. Silver Spring, Maryland.

Nowlin WD, Parker CA (1974) Effects of a cold-air outbreak on shelf waters of the Gulf of Mexico. Journal of Physical Oceanogr. 4:467-486

Pierrot D, Lewis E, and Wallace DWR (2006) MS Excel Program Developed for CO_2 System Calculations. ORNL/CDIAC-105a. https://doi.org/10.3334/CDIAC/otg.CO2SYS_XLS_CDIAC105a

Rezak R, Bright TJ, McGrail DW (1983) Reefs and banks of the northwestern Gulf of Mexico: Their geological, biological and physical dynamics. Final Report, Northern Gulf of Mexico Topographic Features Synthesis. U.S. Dept. of Interior, Minerals Management Service, Contract No. AA851-CT1-55, Dept. of Oceanography, Texas A&M Univ., Tex. Rept. 83-1-T.

Rezak R, Bright TJ, McGrail DW (1985) Reefs and Banks of the Northwestern Gulf of Mexico. John Wiley & Sons, New York.

Rezak R, Gittings SR, Bright TJ (1990) Biotic assemblages and ecological controls on reefs and banks of the northwest Gulf of Mexico. American Zoologist. 30:23–35

Riebesell U, Gattuso JP (2015) Lessons learned from ocean acidification research. Nature Climate Change. 5:12-14

Sabine C, Feely R, Gruber N, Key R, Lee K, Bullister J, Wanninkhof R, Wong C, Wallace D, Tilbrook B, Millero F, Peng T-H, Kozyr A, Ono T, and Rios AF (2004) The Oceanic Sink for Anthropogenic CO_2. Science. 305:367-371

Schneider K, Erez J (2006) The effect of carbonate chemistry on calcification and photosynthesis in the hermatypic coral Acropora eurystoma. Limnol. and Oceanogr. 51:1284–1293

Schmahl GP, Hickerson EL, Precht WF (2008) Biology and Ecology of Coral Reefs and Coral Communities in the Flower Garden Banks Region, Northwestern Gulf of Mexico. Riegl BM, Dodge RE (eds) Coral Reefs of the USA. Coral Reefs of the World, vol 1. Springer, Dordrecht

Shamberger KEF, Lentz SJ, and Cohen AL (2017) Low and variable ecosystem calcification in a coral reef lagoon under natural acidification. Limnol. and Oceanogr. doi:10.1002/lno.10662

Slowey NC, Crowley TJ (1995) Interdecadal variability of Northern Hemisphere circulation recorded by Gulf of Mexico corals. Geophys. Res. Letters. 22:2345-2348

Sutton AJ, et al. (2018) Pacific Marine Environmental Laboratory. Accessed June 22, 2018. www.pmel.noaa.gov/co2/story/Crescent%2BReef

Takahashi T, Sutherland SC, Wanninkhof R, Sweeney C, Feely RA, Chipman DW, Hales B, Friederich G, Chavez F, Sabine C, Watson A, Bakker DCE, Schuster U, Metzl N, Yoshikawa-Inoue H, Ishii M, Midorikawa T, Nojiri Y, Körtzinger A, Steinhoff T, Hoppema M, Olafsson J, Arnarson TS, Tilbrook B, Johannessen T, Olsen A, Bellerby R, Wong CS, Delille B, Bates NR, de Baar HJW (2009) Climatological mean and decadal change in surface ocean pCO, and net sea-air CO flux over the global oceans. Deep Sea Res. Part II: Topical Studies in Oceanogr. 56:8:554-577

Teague WJ, Wijesekera HW, Jarosz E, Fribance DB, Lugo-Fernández A, and Hallock ZR (2013) Current and hydrographic conditions at the East Flower Garden Bank in 2011. Cont. Shelf Res. 63:43-58

van Heuven S, Pierrot D, Lewis E, and Wallace DWR (2009) MATLAB Program Developed for CO_2 System Calculations. ORNL/CDIAC-105b. CDIAC, Oak Ridge National Laboratory, U.S. Department of Energy, Oak Ridge, Tennessee.

Wagner AJ, Slowey NC (2011) Oxygen isotopes in seawater from the Texas-Louisiana Shelf. Bull. of Mar. Sci. 87:1:1-12

Wanninkhof R, Barbero L, Byrne R, Cai WJ, Huang W-J, Zhang J-Z, Baringer M, and Langdon C (2015) Ocean acidification along the Gulf Coast and East Coast of the USA. Cont. Shelf Res. 98:54-71

Weiss RF (1970) The solubility of nitrogen, oxygen and argon in water and seawater. Deep Sea Research and Oceanographic Abstracts. 17:4:721-735, https://doi.org/10.1016/0011-7471(70)90037-9

Weiss RF (1974) Carbon dioxide in water and seawater: the solubility of a non-ideal gas. Marine Chem. 2:3:203-215, https://doi.org/10.1016/0304-4203(74)90015-2

Yates KK, Dufore C, Smiley N, Jackson C, and Halley RB (2007) Diurnal variation of oxygen and carbonate system parameters in Tampa Bay and Florida Bay. Mar. Chem. 104:110-124